TENSILE CREEP OF 2024-T3 ALUMINUM-ALLOY SHEET

UNDER VARYING LOAD CONDITIONS

By

Avraham Berkovits

Thesis submitted to the Graduate Faculty of the

Virginia Polytechnic Institute

in candidacy for the degree of

MASTER OF SCIENCE

in

Engineering Mechanics

March 1960

TENSILE CREEP OF 2024-T3 ALUMINUM-ALLOY SHEET

UNDER VARYING LOAD CONDITIONS

by

Avraham Berkovits

ABSTRACT

Three theories - the time-hardening theory, the strain-hardening
theory, and the life-fraction theory - are investigated in an effort
to predict creep strains under conditions of varying loads from data
obtained at constant load in the range of interest to the structural
designer. A method is presented for computing an equivalent rupture
stress for the varied load case using the life-fraction theory and the
rupture curve for constant stress tests. The analytical methods are
compared with data obtained from 2024-T3 aluminum-alloy sheet under
tensile creep at constant and varying loads.

TENSILE CREEP OF 2024-T3 ALUMINUM-ALLOY SHEET

UNDER VARYING LOAD CONDITIONS

by

Avraham Berkovits

Thesis submitted to the Graduate Faculty of the

Virginia Polytechnic Institute

in candidacy for the degree of

MASTER OF SCIENCE

in

ENGINEERING MECHANICS

March 1960

Blacksburg, Virginia

II. TABLE OF CONTENTS

III. LIST OF FIGURES AND TABLES

- 6 -

IV. NOMENCLATURE

A, A'	constants
B	constant exponent
C	constant, $C = \dfrac{\sigma_r}{A'}$
K	constant
k	constant exponent
N	cycle number
n	constant exponent
q	constant exponent
t	time, hr.
Δt	time increment, hr.
α	constant exponent
ϵ	creep strain, inch/inch
ϵ_o	constant, inch/inch
σ	stress, ksi
σ_o	constant, ksi
σ_e	equivalent rupture stress, ksi

Subscripts:

A, B', B'', B''' designation of points in figure 1

i, j	index notation
m, n	index notation
r	rupture

V. INTRODUCTION

The increasing use of engineering materials under elevated temperature environments in recent years has resulted in greater interest being shown in the creep phenomenon. Considerable information has been published through the years dealing with the creep rupture and creep strain of a multitude of materials under conditions of constant temperature and constant stress or load. Much effort has also been expended in describing the process of creep under such conditions both theoretically and empirically. However, in most cases of actual service stress and temperature vary, and in such cases the use of data obtained under isothermal steady load conditions for design purposes becomes questionable.

For this reason the attention of several investigators (e.g., refs. 1 through 4) has recently been turned toward the problems of creep under varying stresses and temperatures. Creep tests under such conditions fall into three categories: constant stress, variable temperature tests; constant temperature, alternating stress tests - commonly referred to as elevated temperature fatigue; and constant temperature, cyclic stress tests in which the cycle frequency is low enough to allow the exclusion of fatigue considerations. Some investigators have conducted tests in which both stress and temperature were varied simultaneously. The difficulty of analyzing data from such tests is immediately apparent.

This thesis reports on a series of creep tests conducted at the National Aeronautics and Space Administration on strips of 2024-T3 aluminum-alloy sheet material under constant elevated temperature and

cyclic tensile loads. The data obtained are presented and compared with theoretical creep strain and rupture calculations based on data obtained at constant loads from the same sheet. Results are discussed in terms of dislocation and recovery theories.

VI.   THEORETICAL CONSIDERATIONS

It has been pointed out (refs. 5 and 6) that in general the maximum allowable permanent set during creep of structural elements (i.e., creep strain) is on the order of 0.002 inch/inch. This being the case, the structural designer must have at his disposal methods for analytically determining the amount of creep strain to be expected under particular creep conditions. This section will discuss some of the work which has been published in the past dealing with the prediction of creep strain under both constant and varying loads. Some consideration will also be given to the mechanism of creep and recovery, based on dislocation theories; the occasion will arise in the discussion of experimental results to refer to such theories.

A. Constant Stress Creep

Various empirical expressions have been suggested previously for describing the primary and secondary portions of creep curve families. One form suggested in reference 7 is

$$\epsilon = K\sigma^\mu(1 - e^{-qt}) + A\sigma^n t \tag{1}$$

where ϵ is the creep strain, inch/inch

σ is the applied stress, ksi

t is time, hr.

K, α, q, A and n are constants

Equation (1) gives good agreement with experimental data, but is somewhat unwieldly because of the necessity of evaluating five constants.

An expression for constant rate creep suggested in references 8 through 10 takes the form

$$\epsilon = \epsilon_O + A \, t \, \sinh \frac{\sigma}{\sigma_O} \tag{2}$$

where ϵ_O is the total primary creep, inch/inch, and A and σ_O are constants. This equation is inadequate at very short times.

Another expression which has been used (refs. 11 and 12) to predict creep strain takes the form

$$\epsilon = A \, e^{B\sigma} \, t^k \tag{3}$$

where A, B, and k are constants. Although equation (3) agrees well with experimental data in the primary and part of the secondary stages of creep, it has the disadvantage that finite creep strain will be predicted even when the stress is zero.

The form often used by the NASA and others (refs. 13 and 14) to approximate primary and secondary stage creep is a combination of equations (2) and (3)

$$\epsilon = A \, t^k \, \sinh \frac{\sigma}{\sigma_O} \tag{4}$$

(cf., ref. 15) where

   ϵ is creep strain, inch/inch

   σ is applied stress, ksi

   t is time, hr.

   σ_O is a constant, ksi

   k is a constant, dimensionless

   A is a constant, hr.$^{-k}$

Equation (4) has been found to approximate creep data satisfactorily in both the primary and secondary stages of creep, and is the expression

used to describe the experimental results under constant load in
this investigation.

B. Cyclic Load Creep

In the past decade or so the attention of several investigators
has been turned toward theoretical and experimental studies of creep
behavior when the applied stress does not remain constant. An excellent
summary of this work is that of reference 4. Most of the previously
published data on creep under cyclic loading is available there, and only
the theories which were used in the analysis of the present data will
be dealt with here.

Since cyclic loading by definition involves change in stress and
repetitive stress application, investigation of the theories of relaxation
and fatigue with regard to their possible application to the creep
problem would seem feasible (ref. 16). Three such theories are the
time-hardening law, the strain-hardening law and the life-fraction rule.

1. _Time-hardening theory_.- The time-hardening law, based on the
assumption that the annealing process governs during creep, states that
the creep behavior of a material at any stress depends on the time
elapsed. (See ref. 17.) Thus in figure 1, if a creep test is performed
at stress σ_A until the creep strain reaches point A at time t_A,
and the stress is then suddenly changed to σ_B, the ensuing strain rate
will be the same as that at point B', where $t_A = t_B$. The creep curve
will follow the solid line segment A - B' in figure 1.

Using equation (4) to describe the family of creep curves, the time-
hardening theory can be expressed mathematically as follows. Let the
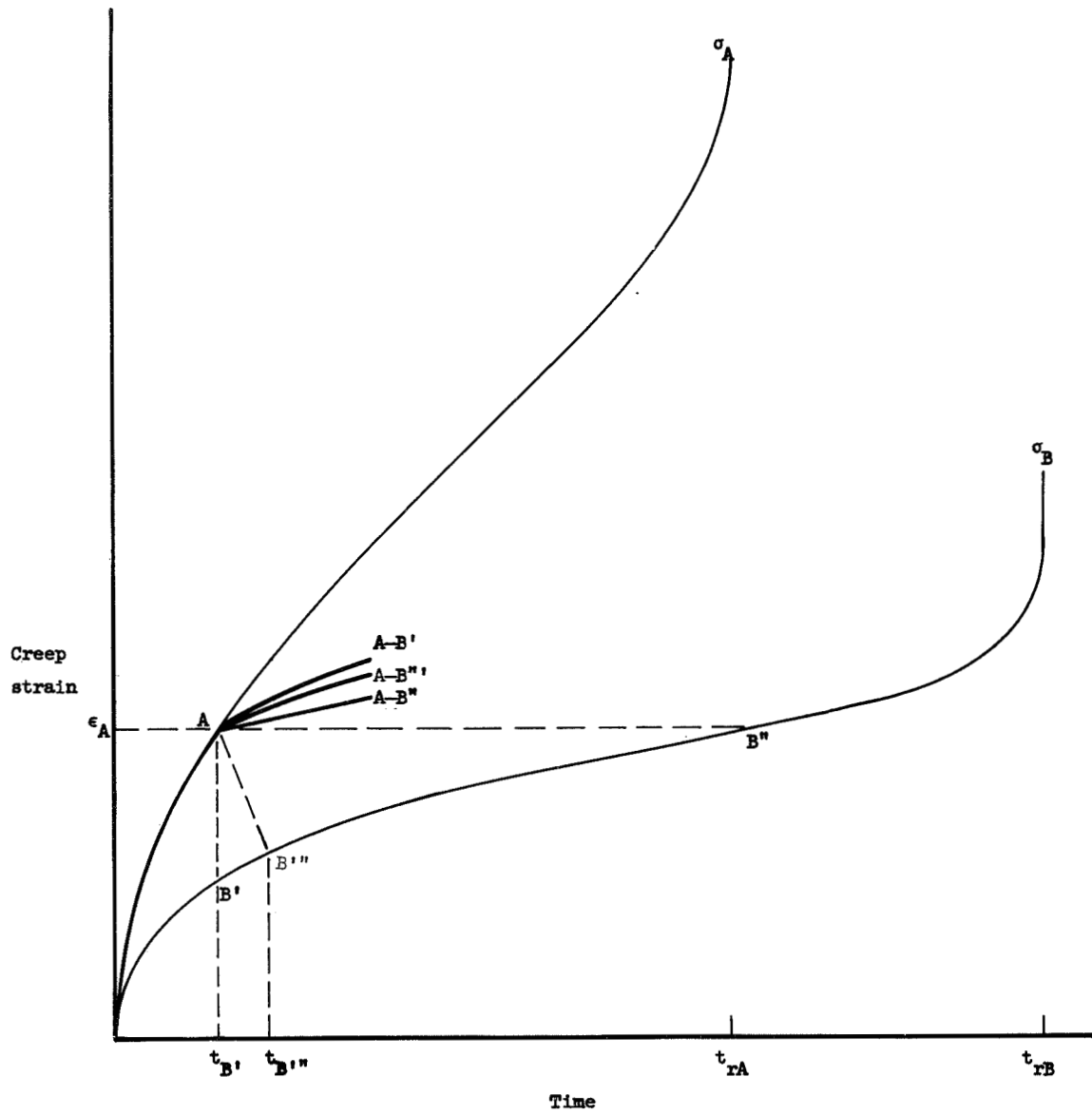
Figure 1.- Comparison of time-hardening, strain-hardening, and life-fraction theories for creep.

creep test begin at stress σ_1 and continue until time t_1. Then at t_1

$$\epsilon_1 = A t_1^k \sinh \frac{\sigma_1}{\sigma_o} \qquad (5)$$

The stress is now changed to σ_2 and the test continues at σ_2 until t_2. At this time

$$\epsilon_2 = A t_1^k \sinh \frac{\sigma_1}{\sigma_o} + A t_2^k \sinh \frac{\sigma_2}{\sigma_o} - A t_1^k \sinh \frac{\sigma_2}{\sigma_o}$$

$$= A \left[t_1^k \sinh \frac{\sigma_1}{\sigma_o} + (t_2^k - t_1^k) \sinh \frac{\sigma_2}{\sigma_o} \right] \qquad (6)$$

Similarly at any stress σ_i and time t_i the total accumulated creep strain predicted by the time-hardening theory is

$$\epsilon_i = A \left[t_1^k \sinh \frac{\sigma_1}{\sigma_o} + (t_2^k - t_1^k) \sinh \frac{\sigma_2}{\sigma_o} + \ldots \right.$$

$$\left. \ldots + (t_i^k - t_{i-1}^k) \sinh \frac{\sigma_i}{\sigma_o} \right]$$

$$= A \sum_{n=1}^{n=i} \left[(t_n^k - t_{n-1}^k) \sinh \frac{\sigma_n}{\sigma_o} \right] \qquad (7)$$

2. Strain-hardening theory.- This theory is founded on the assumption that work-hardening is the governing factor, and states that when the applied stress is changed during a creep test the ensuing creep rate is determined by the amount of creep strain which has already occurred. (See ref. 17.) Thus in figure 1, when the stress is changed at point A, creep continues along the solid line segment A - B" at a rate equal to the creep rate at point B", where $\epsilon_A = \epsilon_{B''}$. In analytical form the creep strain, after changing the stress to σ_2 at t_1 and continuing at σ_2 until t_2, is

$$\epsilon_2 = A \, t_1^{\,k} \sinh \frac{\sigma_1}{\sigma_0} + A \left[t_1 \left(\frac{\sinh \frac{\sigma_1}{\sigma_0}}{\sinh \frac{\sigma_2}{\sigma_0}} \right)^{1/k} + \Delta t_2 \right]^k \sinh \frac{\sigma_2}{\sigma_0}$$

$$- A \, t_1^{\,k} \sinh \frac{\sigma_1}{\sigma_0}$$

$$= A \left[t_1 \left(\frac{\sinh \frac{\sigma_1}{\sigma_0}}{\sinh \frac{\sigma_2}{\sigma_0}} \right)^{1/k} + \Delta t_2 \right]^k \sinh \frac{\sigma_2}{\sigma_0} \qquad (8)$$

where

$$\Delta t_2 = t_2 - t_1$$

and

$$t_1 \left(\frac{\sinh \frac{\sigma_1}{\sigma_0}}{\sinh \frac{\sigma_2}{\sigma_0}} \right)^{1/k}$$

is the time necessary to achieve a strain equal to ϵ_1 at stress σ_2.

Similarly at σ_3 and t_3

$$\epsilon_3 = A \left[\frac{t_1 \left(\sinh \frac{\sigma_1}{\sigma_0} \right)^{1/k} + \Delta t_2 \left(\sinh \frac{\sigma_2}{\sigma_0} \right)^{1/k}}{\left(\sinh \frac{\sigma_3}{\sigma_0} \right)^{1/k}} + \Delta t_3 \right]^k \sinh \frac{\sigma_3}{\sigma_0}$$

$$= A \left[t_1 \sinh^{1/k} \frac{\sigma_1}{\sigma_0} + \Delta t_2 \sinh^{1/k} \frac{\sigma_2}{\sigma_0} + \Delta t_3 \sinh^{1/k} \frac{\sigma_3}{\sigma_0} \right]^k \qquad (9)$$

Thus at any σ_i and t_i, the strain-hardening theory predicts a creep strain

$$\epsilon_i = A \left[\sum_{n=1}^{n=i} \Delta t_n \sinh^{1/k} \frac{\sigma_n}{\sigma_0} \right]^k \qquad (10)$$

Note that equation (10) implies that

$$\Delta t_1 = t_1 - t_0 = t_1$$

3. **Life-fraction rule.-** While the previous theories were originally used for relaxation problems, the life-fraction rule (sometimes referred to as the linear cumulative damage law) was developed by Palmgren and independently by Miner for use in fatigue (refs. 18 and 19). The life-fraction rule assumes that the shape of the creep curve is determined by the fraction of creep life which has been consumed. Thus in figure 1 creep will continue according to this theory from point A along the solid line segment $A - B'''$ parallel to the creep curve at point B'''. The point B''' is determined by the equation

$$t_A/t_{rA} = t_{B'''}/t_{rB} \tag{11}$$

where t_{rA} and t_{rB} are the rupture times at σ_A and σ_B, respectively.

Developing equation (4) in a manner similar to that employed heretofore we obtain

$$c_2 = A\, t_1^k \sinh \frac{\sigma_1}{\sigma_o} + A\left[\left(t_{r2}\frac{\Delta t_1}{t_{r1}} + \Delta t_2\right)^k - \left(t_{r2}\frac{\Delta t_1}{t_{r2}}\right)^k\right]\sinh \frac{\sigma_2}{\sigma_o} \tag{12}$$

and

$$c_i = A\, t_1^k \sinh \frac{\sigma_1}{\sigma_o} + A\left[\left(t_{r2}\frac{\Delta t_1}{t_{r1}} + \Delta t_2\right)^k - \left(t_{r2}\frac{\Delta t_1}{t_{r1}}\right)^k\right]\sinh \frac{\sigma_2}{\sigma_o} +$$

$$A\left[\left(t_{r3}\frac{\Delta t_1}{t_{r1}} + t_{r3}\frac{\Delta t_2}{t_{r2}} + \Delta t_3\right)^k - \left(t_{r3}\frac{\Delta t_1}{t_{r1}} + t_{r3}\frac{\Delta t_2}{t_{r2}}\right)^k\right]\sinh \frac{\sigma_3}{\sigma_o} +$$

$$\dots + A\, t_{ri}^k\left\{\left(\sum_{n=1}^{n=i}\frac{\Delta t_n}{t_{rn}}\right)^k - \left(\sum_{n=1}^{n=i-1}\frac{\Delta t_n}{t_{rn}}\right)^k\right\}\sinh \frac{\sigma_i}{\sigma_o}$$

$$= A\, t_1^k \sinh \frac{\sigma_1}{\sigma_o} + A\sum_{m=2}^{m=i}\left\{t_{rm}^k\left[\left(\sum_{n=1}^{n=m}\frac{\Delta t_n}{t_{rn}}\right)^k - \left(\sum_{n=1}^{n=m-1}\frac{\Delta t_n}{t_{rn}}\right)^k\right]\sinh \frac{\sigma_m}{\sigma_o}\right\} \tag{13}$$

The three theories discussed will be compared, as they appear in equations (7), (10), and (13), with the data obtained in this investigation.

These theories are macroscopic in level and empirical in nature. They give no consideration to the mechanism of creep, or to recovery which might occur when the applied stress is reduced. However, since theory of creep and recovery will be of some importance to the discussion of the present results, a few general comments will be included here.

C. Mechanism of Creep and Recovery

The consensus of opinion among scientists appears to be that the creep process depends on the movement of dislocations within the grains of the material. Excellent discussions and bibliographies of dislocation theory with regard to the creep phenomenon are given in references 20 and 21. The present note is based specifically on the presentation in reference 22, which includes a treatment of effects due to sudden changes in creep stress.

1. _Dislocation movement_.- It is assumed that within the grains of a plastic material there are always a number of Frank-Read dislocation sources, which can be activated to a greater or lesser degree by the application of shear stresses of various magnitudes to the crystals or grains. Furthermore the assumption is made that obstacles of various kinds exist in the paths of the dislocations, and that the stresses required to pass dislocations over or through an obstacle are greater than the source activation stresses.

When stress is applied the dislocations will become activated and move along their glide paths until the front dislocation is stopped by an obstacle. The region between the source and the first obstacle will continue to fill up with dislocations until equilibrium is achieved

between the dislocations and the applied stress, and the dislocations cease to move, or until the energy of the dislocation line becomes sufficient for the first dislocation to overcome the obstacle and the process continues. Eventually, if the applied stress is large enough, sufficient dislocations will be in motion simultaneously to cause finite deformation of the specimen.

2. Creep.- Primary creep occurs in the manner described above. The application of stress activates the dislocation sources and the dislocations begin to move out through the grain boundaries. However, the deformation taking place in the grain boundaries causes the boundaries to be reoriented in positions less favorable to the passage of further dislocations. As a result of this work-hardening the creep rate decreases and a lower equilibrium rate is soon reached at which the average number of dislocations per unit area of glide plane becomes constant, and the sources activate dislocations at the same rate at which the dislocations leave the glide plane. This is the phenomenon known as steady creep.

3. Creep recovery.- If the specimen is unloaded after steady state creep has been established during a test, the immediate dislocation density is much higher than the new equilibrium density at zero stress. The excess dislocations will be annihilated by mutual attraction or by driving each other out through the boundaries of the specimen or back into the sources. In this manner the properties of the material will be caused to change, and conceivably reverse creep could also occur.

4. Effect of stress change.- The effects of a finite increase or decrease in creep stress can be explained in terms of what has been

said above about the transient creep and recovery phenomena. With
an increase in stress the dislocation sources become more active,
resulting in a considerably higher creep rate until the material is
again sufficiently work hardened at the grain boundaries to achieve
the new equilibrium or steady state creep rate.

When the stress is decreased the number of dislocations between
any two obstacles will be larger than the new equilibrium number. The
surplus dislocations in the region next to the surface will leave the
material rather quickly, but they will cause a negligible amount of
strain because they are relatively few in number. Eventually the
new equilibrium dislocation density will be achieved in the outer
region and the dislocations will continue to leave this region at the
new equilibrium rate. However, until this condition is reached no
dislocations can leave the next inner region and enter the outer region,
because the dislocation density there is still above normal for the
applied stress. When dislocations begin to move in the second region,
this region is also oversaturated with dislocations and it will not be
fed from the third region until after equilibrium is again achieved.

This process continues for the regions between every two obstacles
in turn until the new equilibrium dislocation density is reached every-
where between the source and the material surface. Thus although each
moving dislocation travels at a rate faster than normal for the new
stress, few dislocations are moving at any given time and the resulting
creep strain is extremely small until steady state creep recommences
throughout the specimen.

Unfortunately most of the mathematical analysis which has been applied to the calculation of strain under varying load creep conditions has been on the atomic level, and is considered to be beyond the scope of the present investigation. Some empirical methods have been developed for special cases (e.g., ref. 23), but they do not appear to be readily applicable to the tests reported herein.

VII.   TEST SPECIMENS AND EQUIPMENT

A. Specimens

Fifty tensile test blanks were cut from a sheet of 2024-T3 aluminum alloy of 0.125 inch nominal thickness. The length of blanks was 24 inches, oriented in the rolling direction of the sheet; they were 1.00 inch in width. The width of each specimen was reduced to 0.500 inch along a 2.00-inch gage length in the middle section. The specimens were carefully measured and the average areas in the gage length were tabulated. (See table 1.)

B. Equipment

Two creep testing machines were used in this investigation. The machine used for the majority of the constant load creep tests is a conventional dead weight beam-loading type of creep testing machine. The second is a beam-loading machine designed and built at NASA (fig. 2) and equipped to apply loads to the specimen using either a weight cage, a hydraulic cylinder or both. This machine was used to perform stress-strain tests and creep tests under cyclic loading.

The furnaces installed in both testing machines are automatically controlled, and are capable of maintaining the test temperature of 400° F with an accuracy of $\pm 2^\circ$ F. The temperature gradient over the gage length of the specimen during all tests was less than $\pm 2\text{-}1/2^\circ$ F, the accuracy of the temperature recorders used for the program.

The extensometer used to measure strain is shown in figure 3. It consists of two microformers mounted at one end of pivoted strain transfer devices. Extensometer rods clamped to the upper and lower gage points

TABLE 1.   AVERAGE GAGE-LENGTH AREAS OF TEST SPECIMENS

| Specimen no.	Area, in.^{2}	Specimen no.	Area, in.^{2}
1	0.0627	26	0.0626
2	.0625	27	.0619
3	.0625	28	.0623
4	.0624	29	.0625
5	.0625	30	.0627
6	.0628	31	.0629
7	.0625	32	.0628
8	.0630	33	.0625
9	.0625	34	.0628
10	.0625	35	.0628
11	.0624	36	.0624
12	.0624	37	.0625
13	.0625	38	.0628
14	.0625	39	.0627
15	.0623	40	.0626
16	.0620	41	.0626
17	.0626	42	.0630
18	.0624	43	.0628
19	.0625	44	.0627
20	.0628	45	.0626
21	.0626	46	.0622
22	.0628	47	.0619
23	.0628	48	.0626
24	.0625	49	.0625
25	.0622	50	.0626
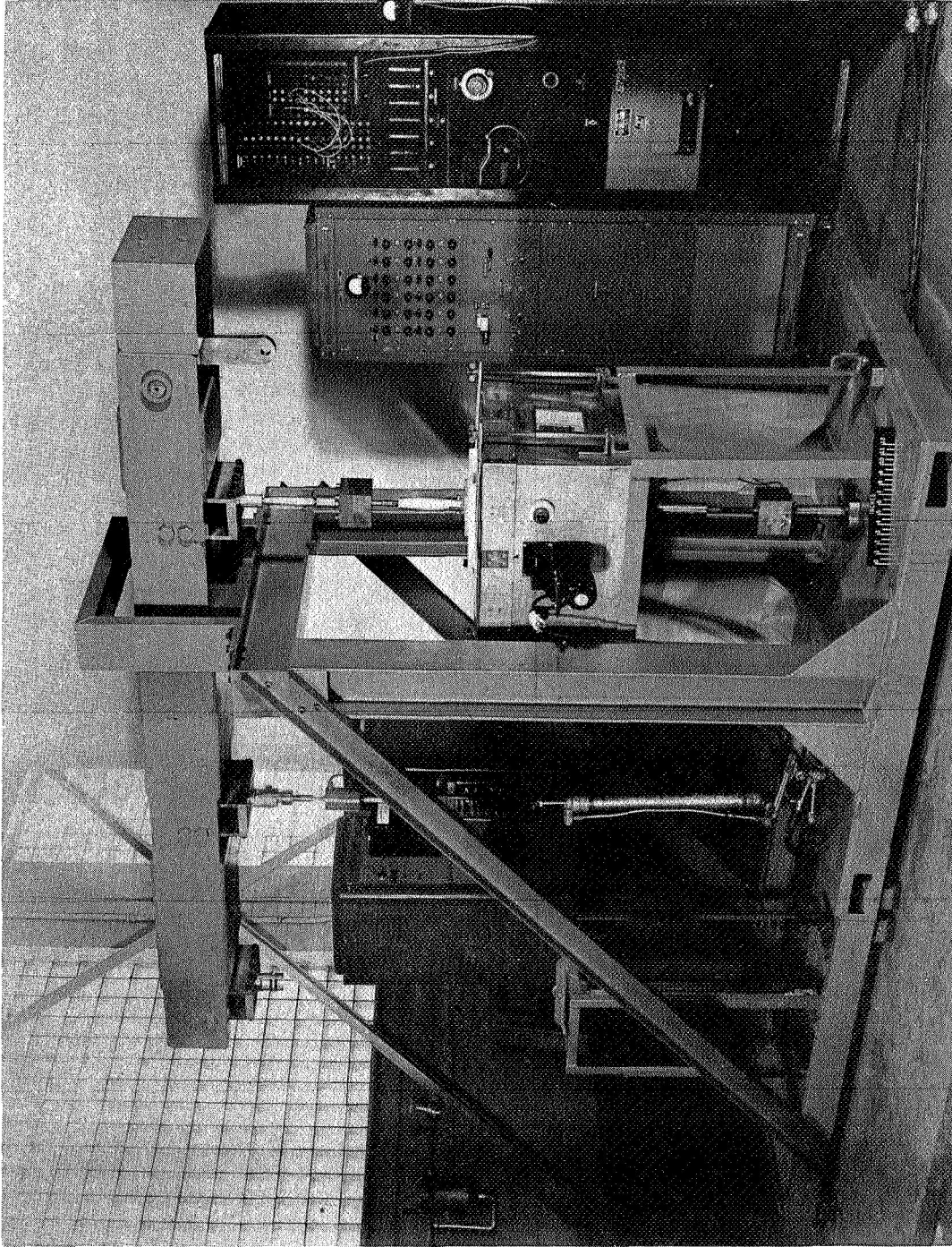
Figure 2.- Variable load creep testing machine.   L-59-7943
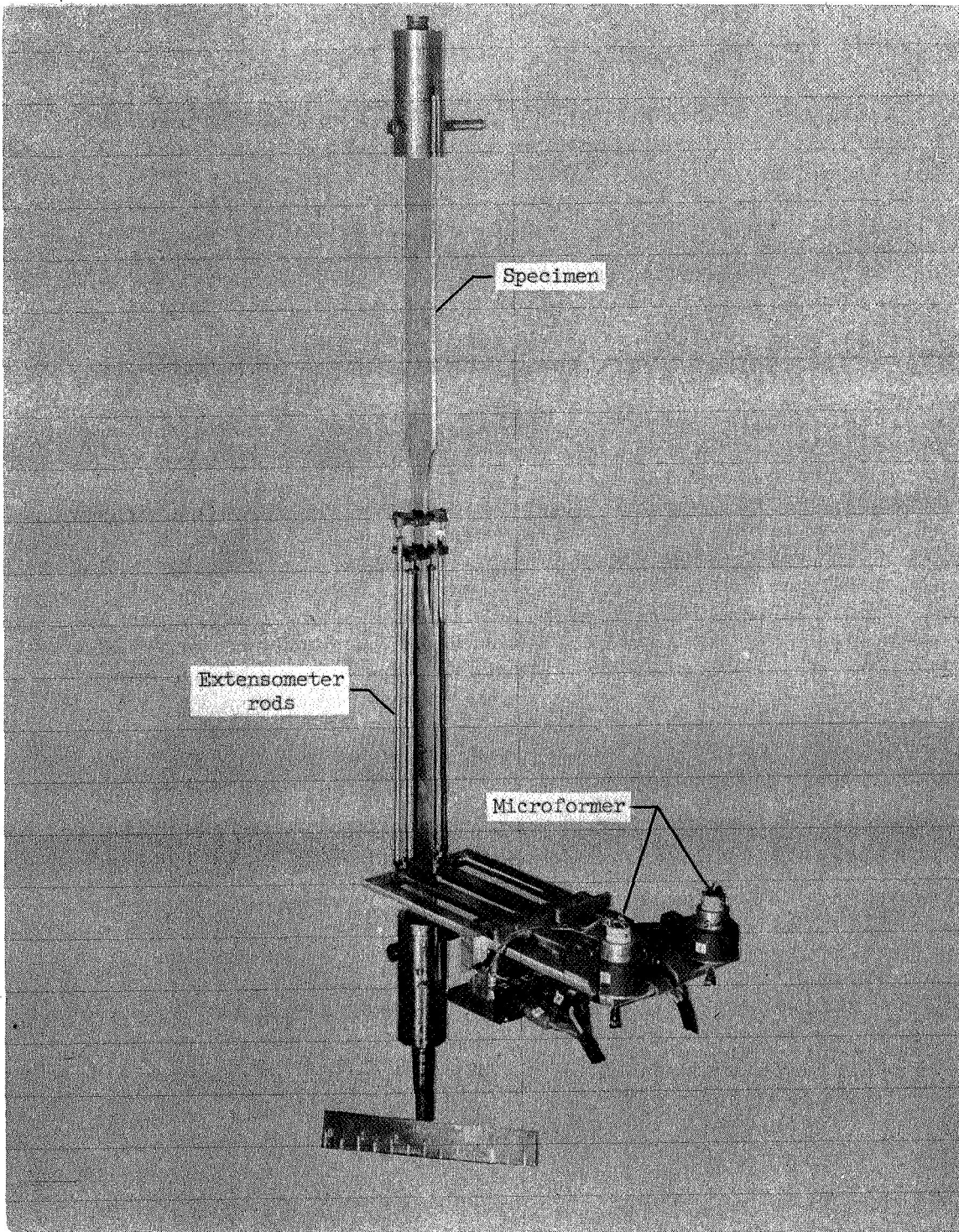
Figure 3.- Extensometer mounted on test specimen.   L-85104.1

on the specimen rest in small holes at the other end of the transfer
devices. One strain transfer device is installed on either side of
the specimen so that strain readings can be electrically averaged
and thus any bending effects eliminated. In this way elongation of
the test specimen is transferred from the gage points through the system
to the microformers, which measure the relative motion of the gage
points. Strain readings from the microformers were recorded auto-
graphically on a previously calibrated time-drive recorder. This
recorder appears on the right in the photograph of the control and recording
equipment of figure 4.

The system diagram of the load programing equipment used for
controlling cyclic loads appears in figure 5. The programer is fed
by a 12-volt de Nobatron power supply unit and contains ten channels
with which it can control from one to ten step loads per cycle
(left center in fig. 4). Each channel to be used is set prior to
the test at the selected load and time duration. The duration of each
step in the cycle can be varied from 0.1 minute to 99.9 minutes.
The cycles may be repetitive, and random cycling can also be programed.
An additional channel is available for the purpose of conducting stress-
strain tests using the same equipment.

The load programer controls a Moog electro-hydraulic servovalve,
which operates at a pressure of 1500 psi and has a capacity of seven
gallons/minute. The servovalve is supplied by a five gallons/minute
2000 psi capacity hydraulic pump, and input pressure to the servovalve
is maintained at 1500 psi by a pressure control valve. During operation
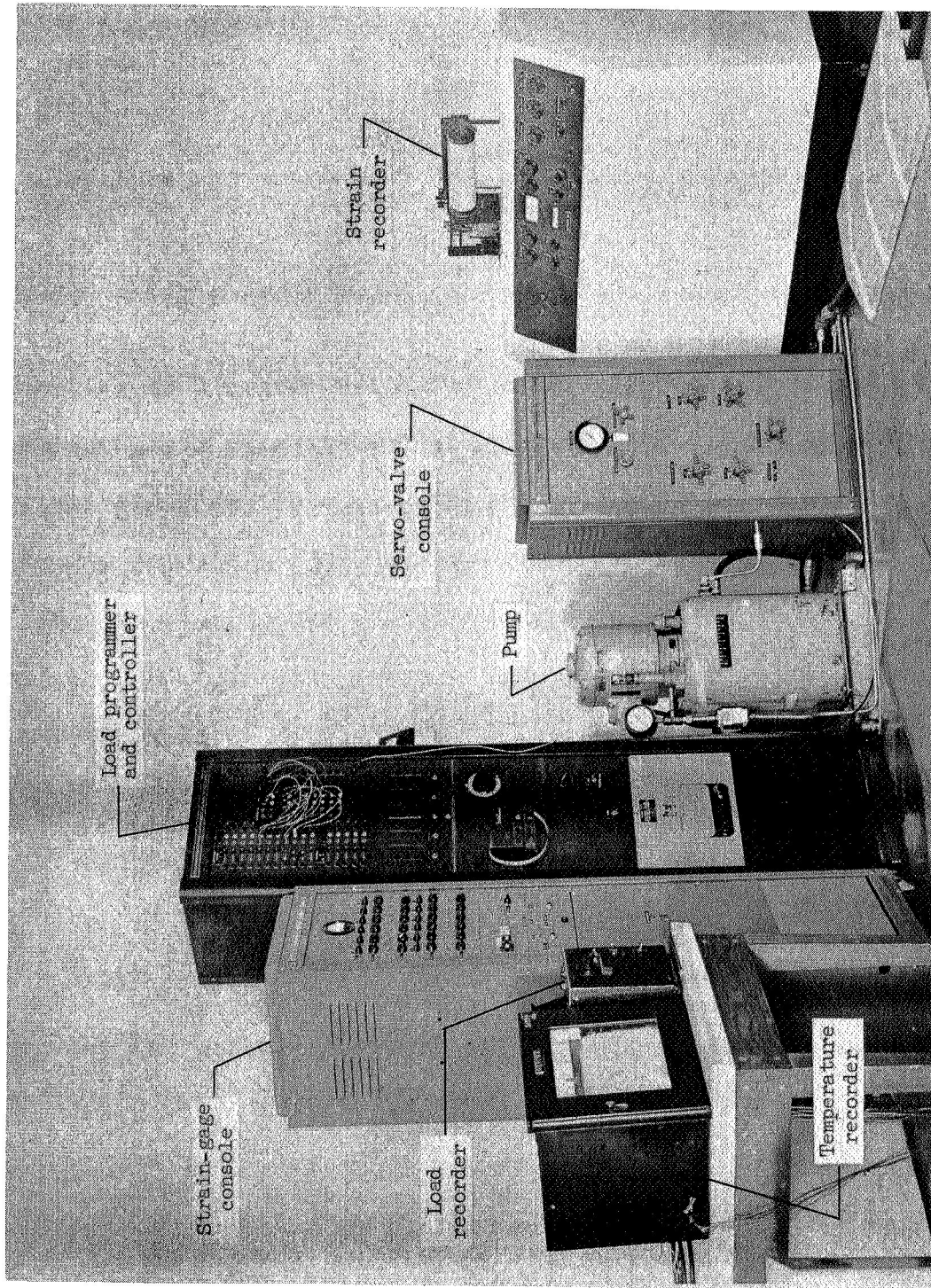the servovalve receives an electric signal from the programer through

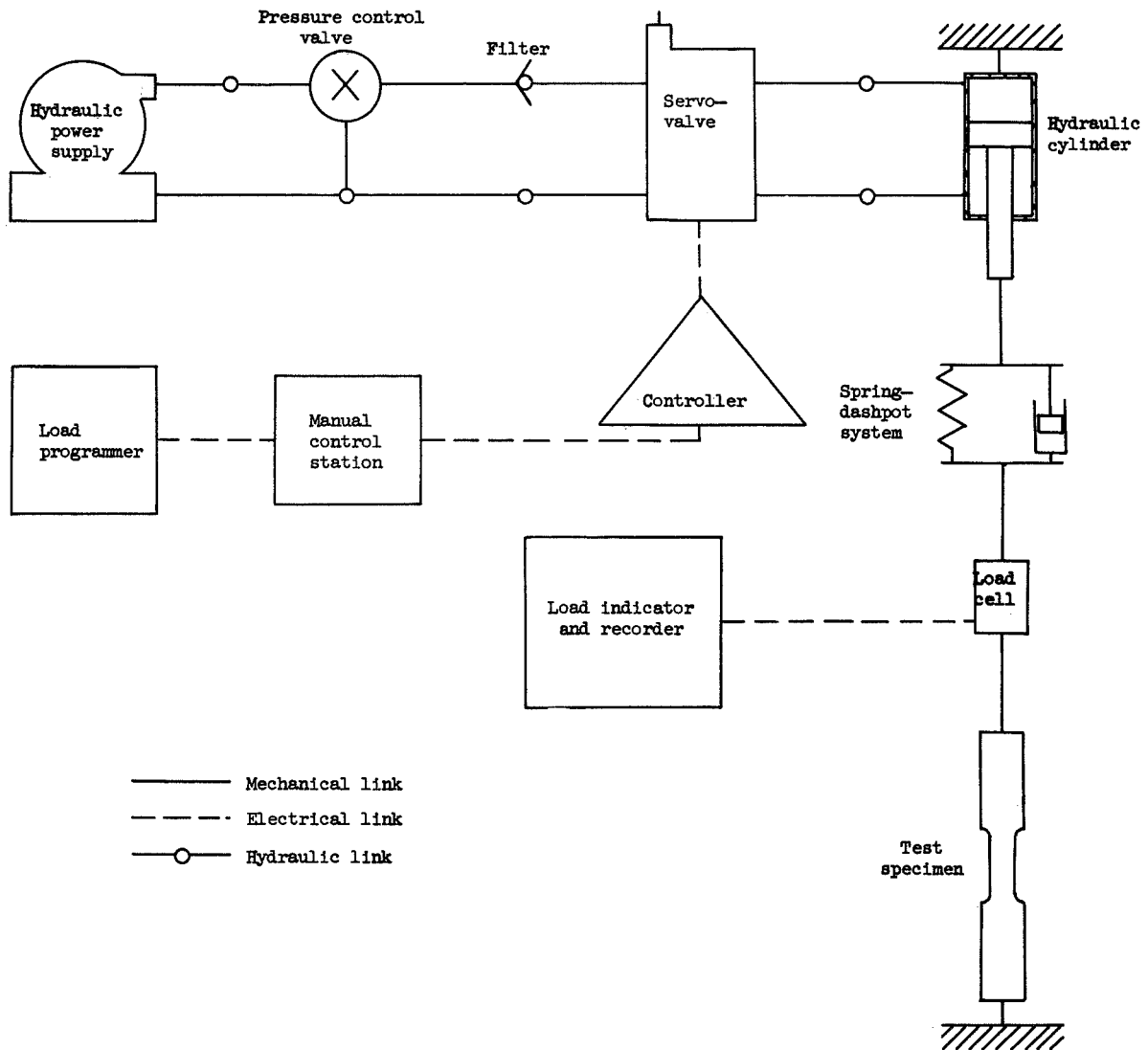Figure 4.- Control and recording equipment.   L-59-4275.1

Figure 5.- System diagram of the load control system.

the controller, and transforms it into a pressure difference across
the piston in the hydraulic loading cylinder, which applied load
to the test specimen. In order to allow a greater oil flow in the system
for a finite change in load, a mechanical spring-dashpot system was
installed in series with the loading cylinder.

The major drawback of the load programing system used is the lack
of automatic feed-back and comparison networks between the load cell
and the controller. However, frequent monitoring of the autographic
load recorder and manual adjustment of the load settings on the programer
permit control of the load levels ±1 percent of the desired values.

VIII. TEST PROCEDURE

All tests were performed at a temperature of 400° F, and each creep specimen was exposed to the test temperature 0.5 hour prior to the application of load. The test equipment was energized at least 45 minutes before the beginning of each test, in order to allow components in the various electrical circuits to warm up, and to permit the oil in the pump reservoir to reach the stable operating temperature.

A. Stress-Strain Tests

Material stress-strain tests were performed at 400° F over the range of exposure times covered by the ensuing creep tests. Tests were conducted at the following exposure times: 0.5, 2, 5, 20, and 50 hours. The specimens used in these tests were exposed for 0.5 hour less than the required exposure times in a large annealing furnace. The last 0.5 hour of exposure to temperature occurred with the specimens in the testing machine immediately prior to performing the test. Load and strain were recorded simultaneously during each test with a Miller oscillograph.

B. Constant Load Creep Tests

Twenty-two specimens were subjected to conventional tensile creep tests in order to obtain a complete set of constant load creep data. Such creep results were necessary for purposes of comparison and calculation for the varying load creep tests. At least two tests were conducted at each stress level over a range of stresses from 10 ksi to 50 ksi. One test was also performed under 55 ksi applied stress, but no strain record was made.

Most of these tests were conducted in the conventional creep testing machine, which operates continuously. Several tests, however, were performed using the other testing machine. This machine cannot be operated continuously and it was necessary to unload and cool the specimen at the end of each day. The effects of this overnight shutdown were compared with data obtained from the conventional testing machine.

Because of the long times involved, creep tests performed at low stresses (i.e., 25 ksi and below) were not prolonged until rupture occurred. These tests were discontinued after appreciable creep strain had been recorded.

C. Varied Load Creep Tests

Stresses and times at stress per cycle for the varied load creep tests are presented in table 2. Stress levels between 30 ksi and 45 ksi were chosen for these tests in order to achieve rupture within reasonable times. The tests consisted of repetitive cycles of equal duration with either two or three distinct step loads in each cycle. Under each stress-time condition investigated at least one test was performed with the load steps in ascending order in the cycle, and at least one test in the opposite order. This procedure afforded a direct indication of the influence of the order of stress application on the creep behavior of the material.

Several creep tests were conducted using two load levels and essentially one loading cycle. After exposure of the specimen to the test temperature of 400° F for 0.5 hour the first stress was applied using dead weight loading, and the test was allowed to proceed until

TABLE 2. CYCLIC LOAD CREEP TESTS

(a) Single-Cycle Tests

No.	σ_1, ksi	Δt_1, hr.	σ_2, ksi	Δt_2
31	40	4.0	45	to rupture
32	45	1.1	40	to rupture
33	45	1.1	40	to rupture
34	30	50.5	40	to rupture
35	40	4.0	30	to rupture
36	40	5.0	30	to rupture
37	40	6.5	30	to rupture

(b) Two-Step Multicyclic Tests

No.	σ_1, ksi	Δt_1, hr.	σ_2, ksi	Δt_2, hr.
38	41.3	0.100	46.3	0.100
39	46.3	.100	41.3	.100
40	41.3	.157	46.3	.043
41	46.3	.043	41.3	.157
42	31.3	.200	41.3	.200
43	41.3	.200	31.3	.200
44	31.3	.927	41.3	.073
45	41.3	.073	31.3	.927

(c) Three-Step Multicyclic Tests

No.	σ_1, ksi	Δt_1, hr.	σ_2, ksi	Δt_2, hr.	σ_3, ksi	Δt_3, hr.
46	31.3	0.200	36.3	0.200	41.3	0.200
47	41.4	.200	36.4	.200	31.4	.200
48	31.3	.730	36.3	.212	41.3	.058
49	31.3	.730	36.3	.212	41.3	.058
50	41.3	.058	36.3	.212	31.3	.730

approximately half of the rupture time at the applied stress had elapsed. Weights were then added or removed as required to achieve the second stress, and the test continued at this load level until rupture of the test specimen occurred. These tests were performed in the conventional testing machine, and continued uninterruptedly until failure occured. This type of test will be referred to as single cycle tests hereafter.

The majority of the cyclic load creep tests were performed in the other testing machine, using the load programing equipment. This entailed unloading and cooling of the specimen at the end of each day of testing.

The stress cycles used were of such duration that many cycles were necessary before failure occurred. Two types of load-time histories were used: equal time cycles, in which the durations of application of all load steps in the cycle were equal; and equal damage cycles, in which the length of time at any load was such that the ratio of the time per cycle spent at that load to the constant load rupture time at that load was approximately a constant for all loads.

IX. RESULTS AND DISCUSSION

A. Stress-Strain Results

The results of the stress-strain tests are reported in table 3 and the stress-strain curves are shown in figure 6. Little need be said concerning these data other than that the material demonstrated gradual strengthening with exposure with a peak yield strength at about two hours, followed by the overaging characteristic of 2024-T3 aluminum alloy at elevated temperatures. The short time material properties of the sheet were in good agreement with previously published data (cf. the compression test results of ref. 24).

B. Constant Stress Creep

Creep and rupture data are given in table 4, and creep strain is plotted against time in figure 7. The effect of unloading and cooling overnight during a test proved to be negligible.

It will be noted in figure 7 that the creep curves all have approximately the same slope on a logarithmic plot, until creep-strain values of approximately 0.005 inch/inch have been achieved. This suggests that equation (4) should fit the creep data satisfactorily. The constants in equation (4) were evaluated and the creep expression was found to be

$$\epsilon = (6.8 \times 10^{-5})t^{1/2} \sinh \frac{\sigma}{9.3} \tag{14}$$

Stresses and rupture times for the creep tests are plotted in figure 8. By crossplotting figure 7 as stress against time for various constant creep strains, it is found that the resulting curves are parallel.

TABLE 3. STRESS-STRAIN DATA

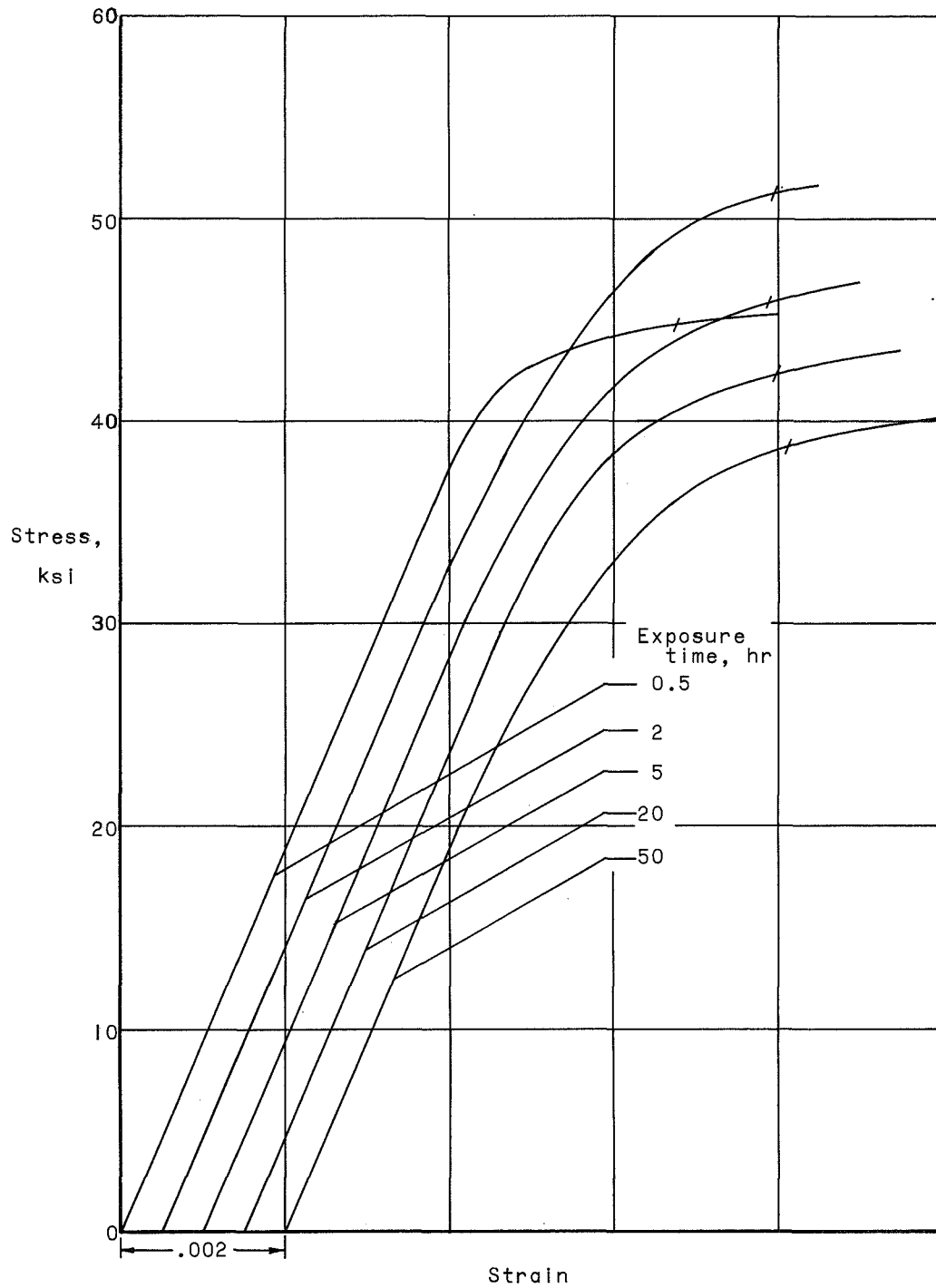| No.	Exposure time, hr.	Young's modulus, psi	Yield stress, psi
1	0.5	9.4×10^6	44.9
2	0.5	9.4	44.7
3	2.0	9.4	51.3
4	5.0	9.4	45.8
5	20.0	9.4	42.6
6	20.0	9.4	42.3
7	50.0	9.4	38.9
8	50.0	9.4	38.8

Figure 6.- Experimental tensile stress-strain curves for 2024-T3 aluminum-alloy sheet at 400° F.

TABLE 4.   CONSTANT LOAD RUPTURE DATA

No.	σ, ksi	Rupture time, hr.
9	10	Test stopped at 90.00
10	10	Test stopped at 150.00
11	10	Test stopped at 46.00
12	15	Test stopped at 66.00
13	15	Test stopped at 55.00
14	20	Test stopped at 66.00
15	20	Test stopped at 45.00
16	25	Test stopped at 53.00
17	25	Test stopped at 45.00
18	25	Test stopped at 50.00
19	30	101.00
20	30	63.90
21	35	62.40
22	35	24.00
23	40	6.50
24	40	9.40
25	45	1.33
26	45	2.18
27	50	0.94
28	50	1.75
29	50	.72
30	55	.16
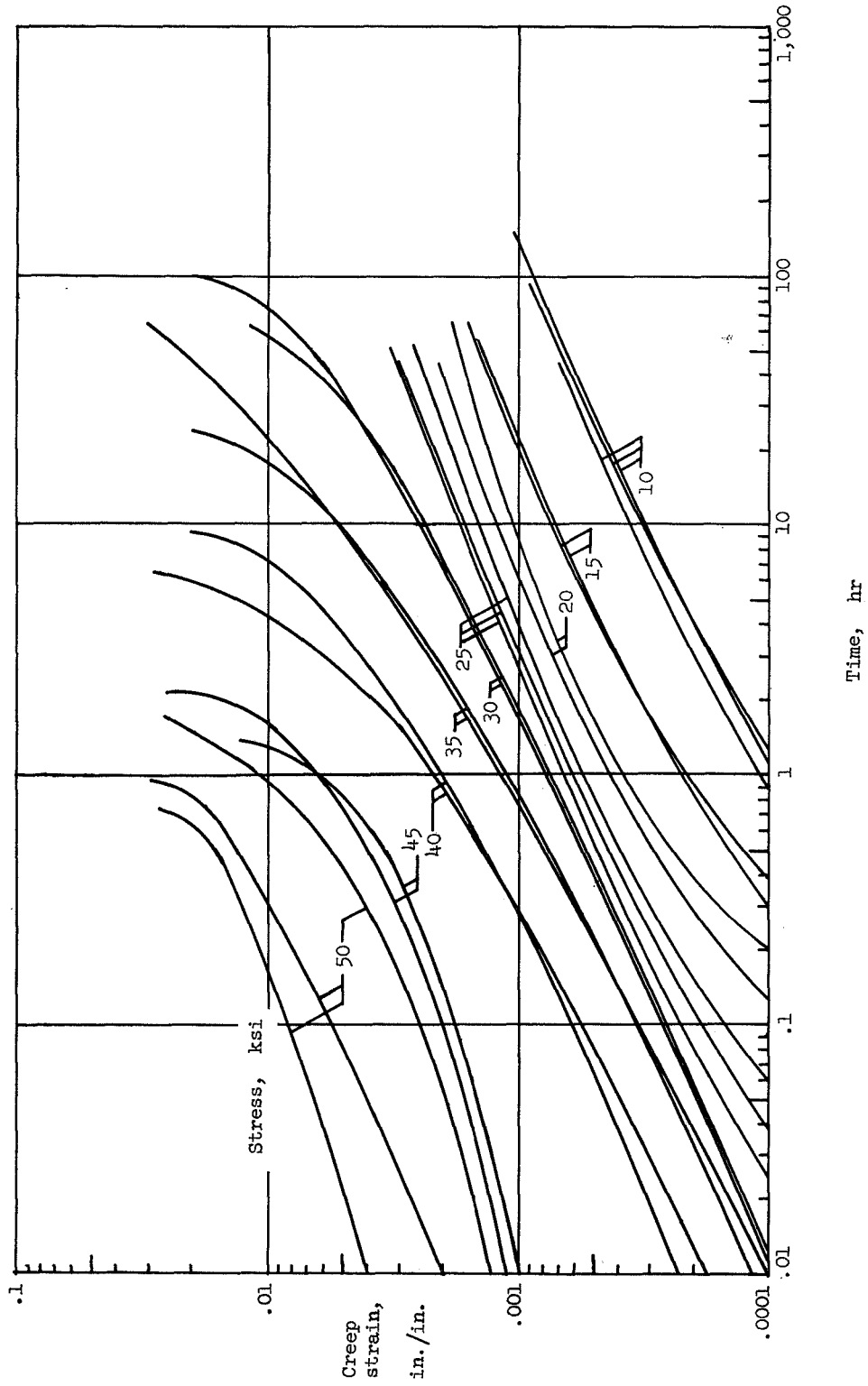
Figure 7.- Experimental tensile creep curves for 2024-T3 aluminum-alloy sheet at 400° F; 0.5-hour exposure prior to test.
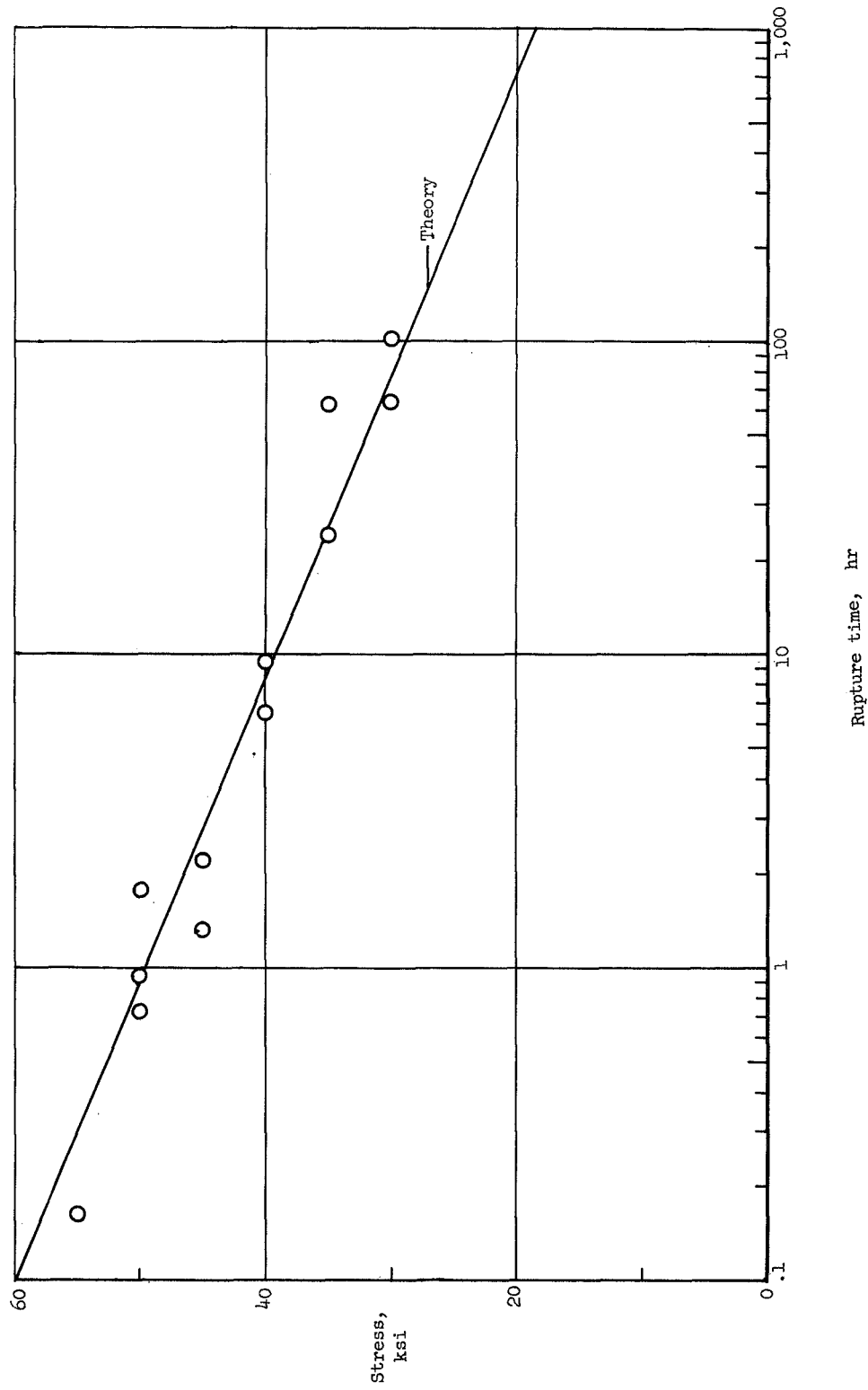
Figure 8.- Creep rupture time of 2024-T3 aluminum-alloy sheet at 400° F under constant load.

This implies that an expression of the form of equation (4) can be used to describe the rupture curve, as well as the creep curves of the material, if the appropriate value for A is substituted. If the creep rupture strain is assumed to be a constant (cf., fig. 7), the rupture curve expression is of the form

$$\epsilon_r = A' \ t_r^k \ \sinh \frac{\sigma}{\sigma_0} \tag{15}$$

where ϵ_r is creep strain at rupture (a constant), t_r is rupture time, A' is the new constant in equation (14), and the other symbols are as before. Solving for rupture time in terms of stress

$$t_r = C/\sinh^{1/k}\left(\frac{\sigma}{\sigma_0}\right) \tag{16}$$

where

$$C = (\epsilon_r/A')^{1/k}$$

Thus in the case of figure 8

$$t_r = 1.2 \times 10^4/\sinh^2\left(\frac{\sigma}{9.3}\right) \tag{17}$$

We will have occasion to refer to this equation again subsequently.

The creep curves of figure 9 were plotted using equation (14) for the straight line portion representing the primary and secondary creep stages, and equation (17) for the failure points. The curved portions of the curves were approximated by referring to figure 7. The dashed line segments represent extrapolation beyond the range of the experimental results.
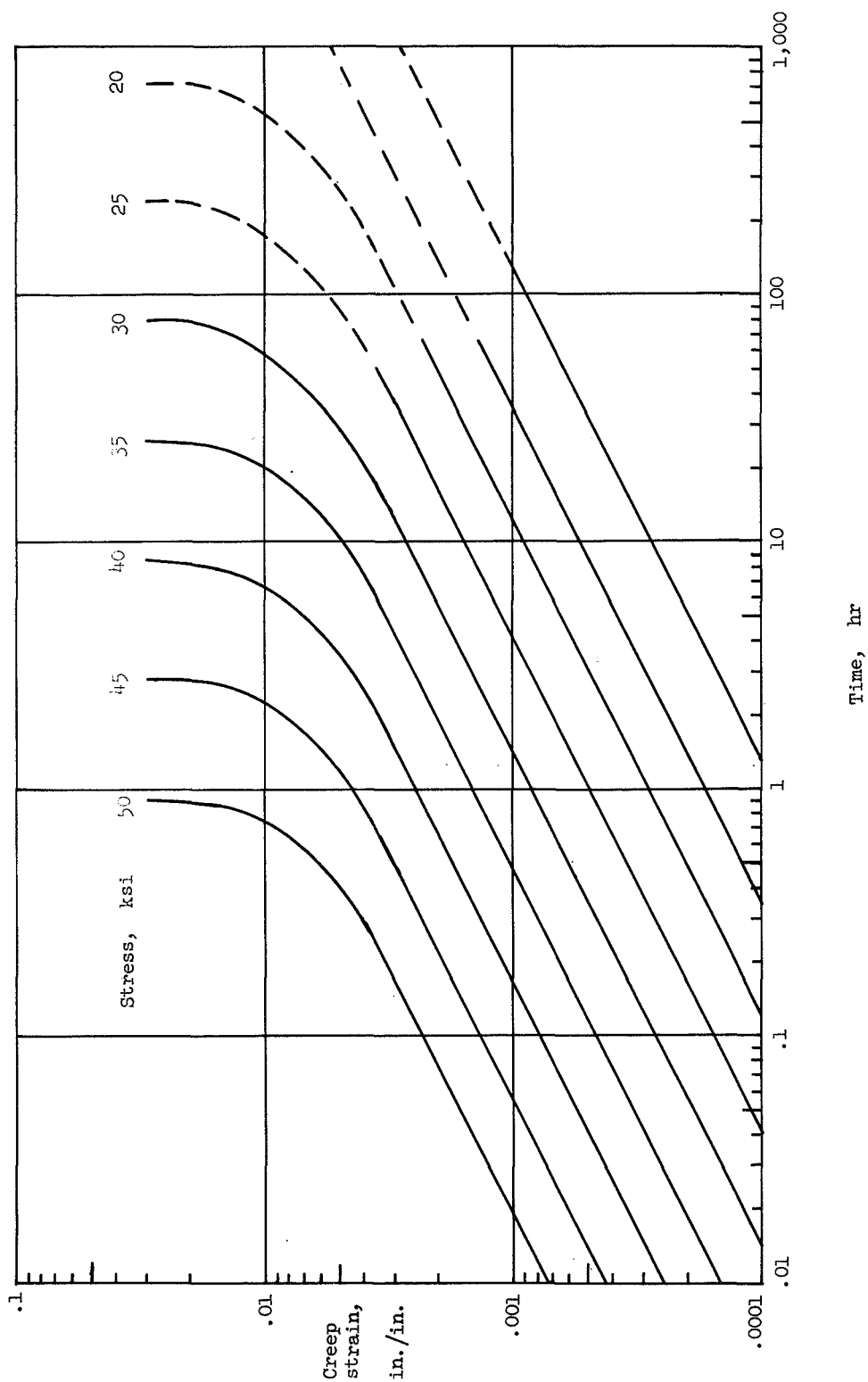
Figure 9.- Theoretical creep curves plotted using equations (14) and (17).

C. Creep Under Varied Loads

1. <u>Creep strain</u>.- The results of the creep tests under varied loads are presented in figures 10 through 24. In each case the constant stress creep curves for the stresses involved are replotted from figure 9.

Figures 10 and 11 show the results of the single cycle creep tests. The point at which the load was changed is apparent in each test. An increase in stress was marked by a large increase in strain rate, and failure of the specimen was imminent. On the other hand note that a decrease in stress caused considerable delay of the creep process in every case. In every single-cycle test in which the higher load was applied first, failure occurred much later than would have been expected had the lower stress been applied throughout the entire test. The high load was applied for three different times during test numbers 35, 36, and 37 (fig. 11) in order to show how the recovery rate is affected by time.

No attempt was made to predict creep strain during the single-cycle tests by using the various theories discussed above, because the point of load change was generally beyond the region in which the creep equation used (eq. (14)) reasonably described the creep curve family.

The results of the multicyclic creep tests are shown in figures 12 through 24. Figures 12 through 19 contain the data obtained from tests in which two stress levels were used; in figures 20 through 24 appear results from the three-step tests. Dashed curves have been drawn through the experimental points for each test to indicate the general trend of the test.

Each of the multicyclic creep tests was compared with time-hardening, strain-hardening and life-fraction theories as represented by
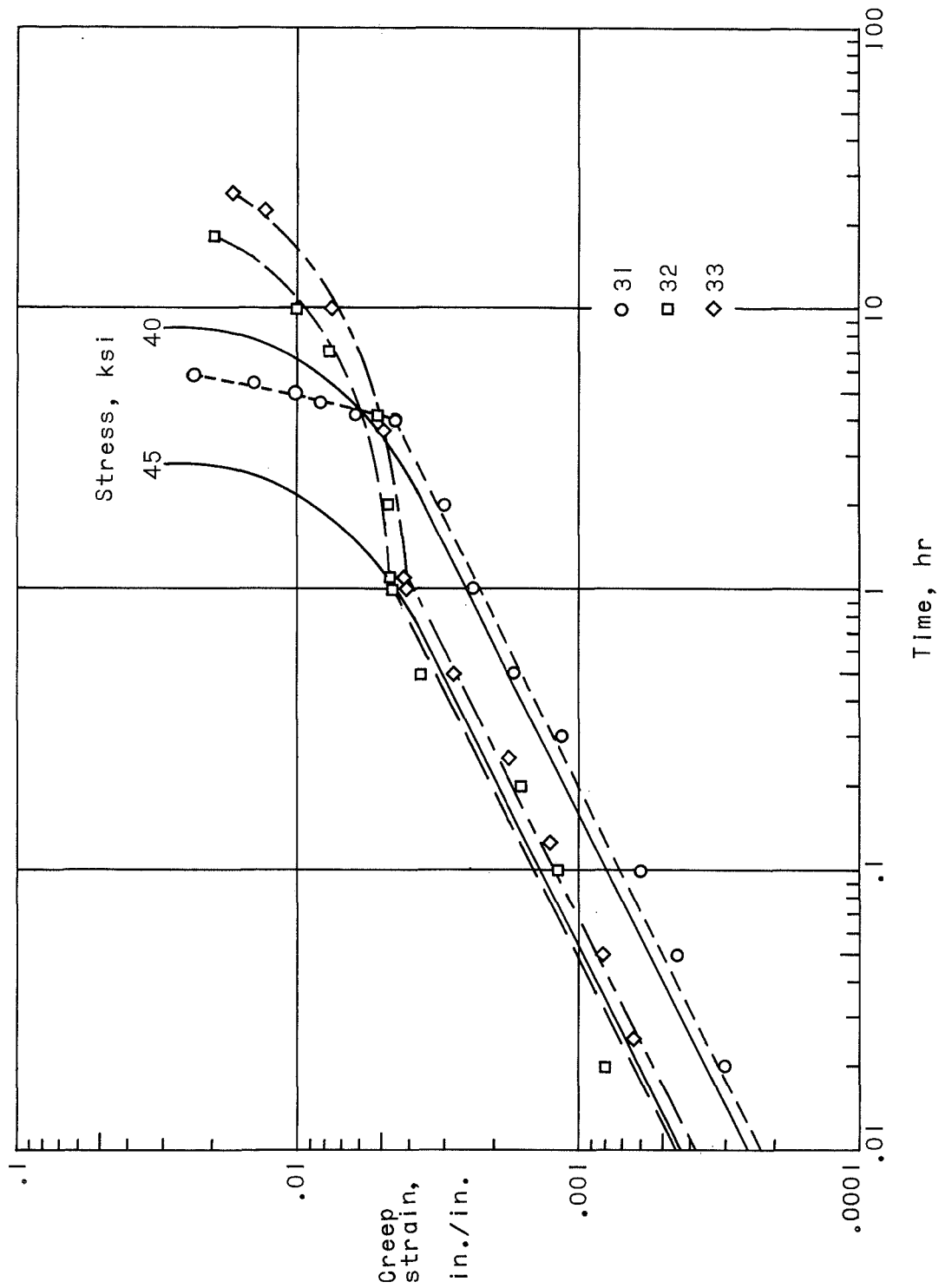
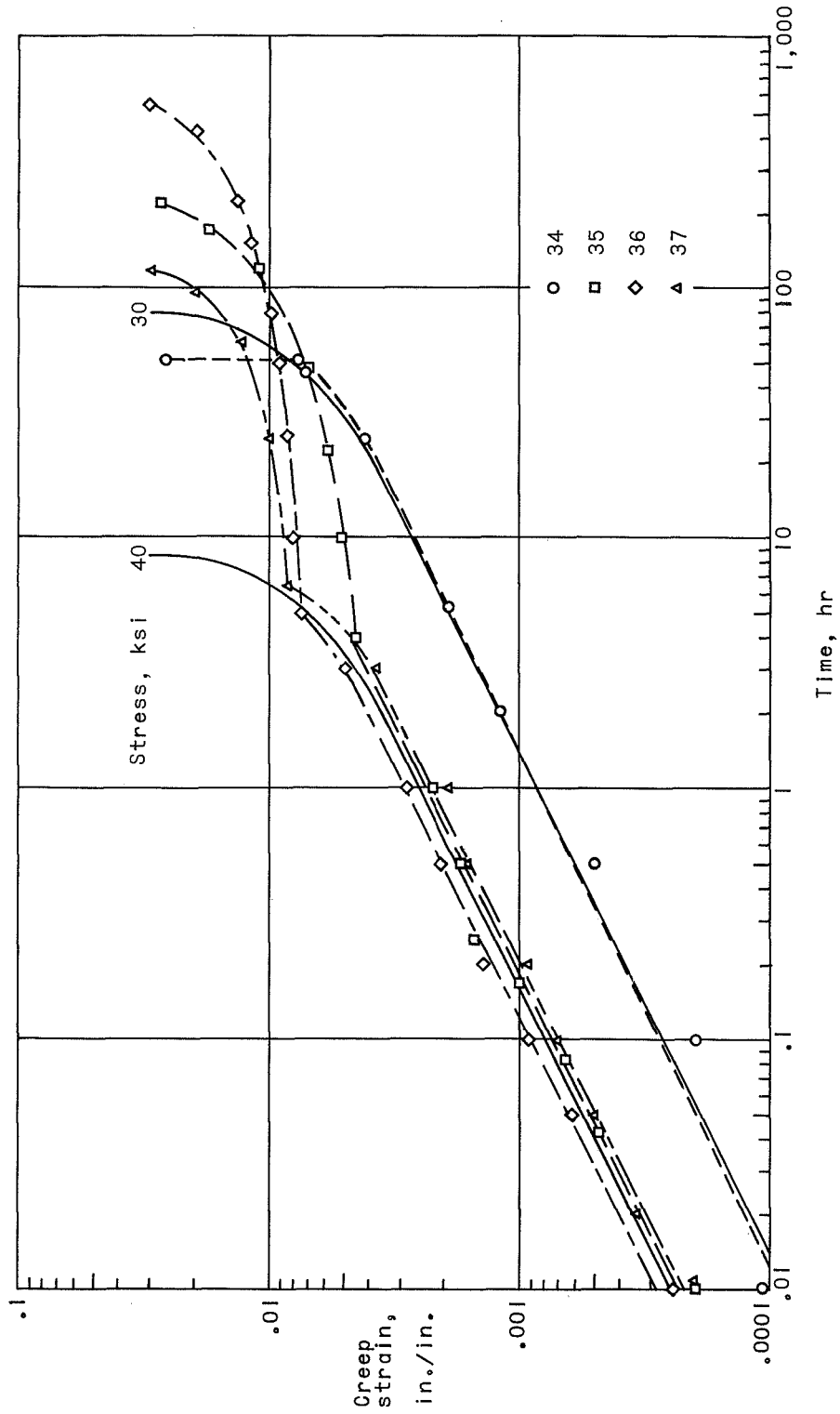Figure 10.- Single cycle creep curves; tests number 31-33.

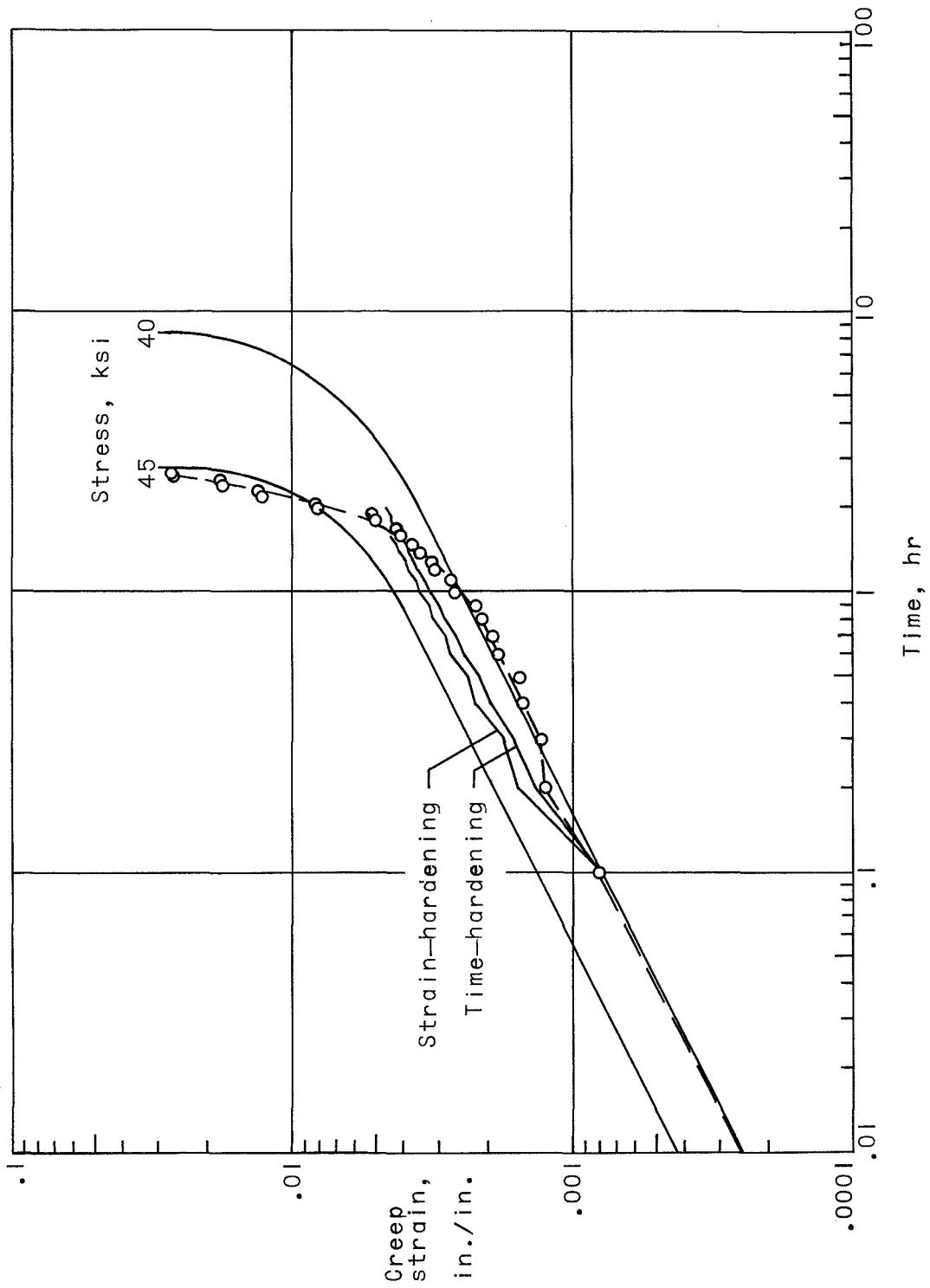Figure 11.- Single cycle creep curves; tests number 34-37.

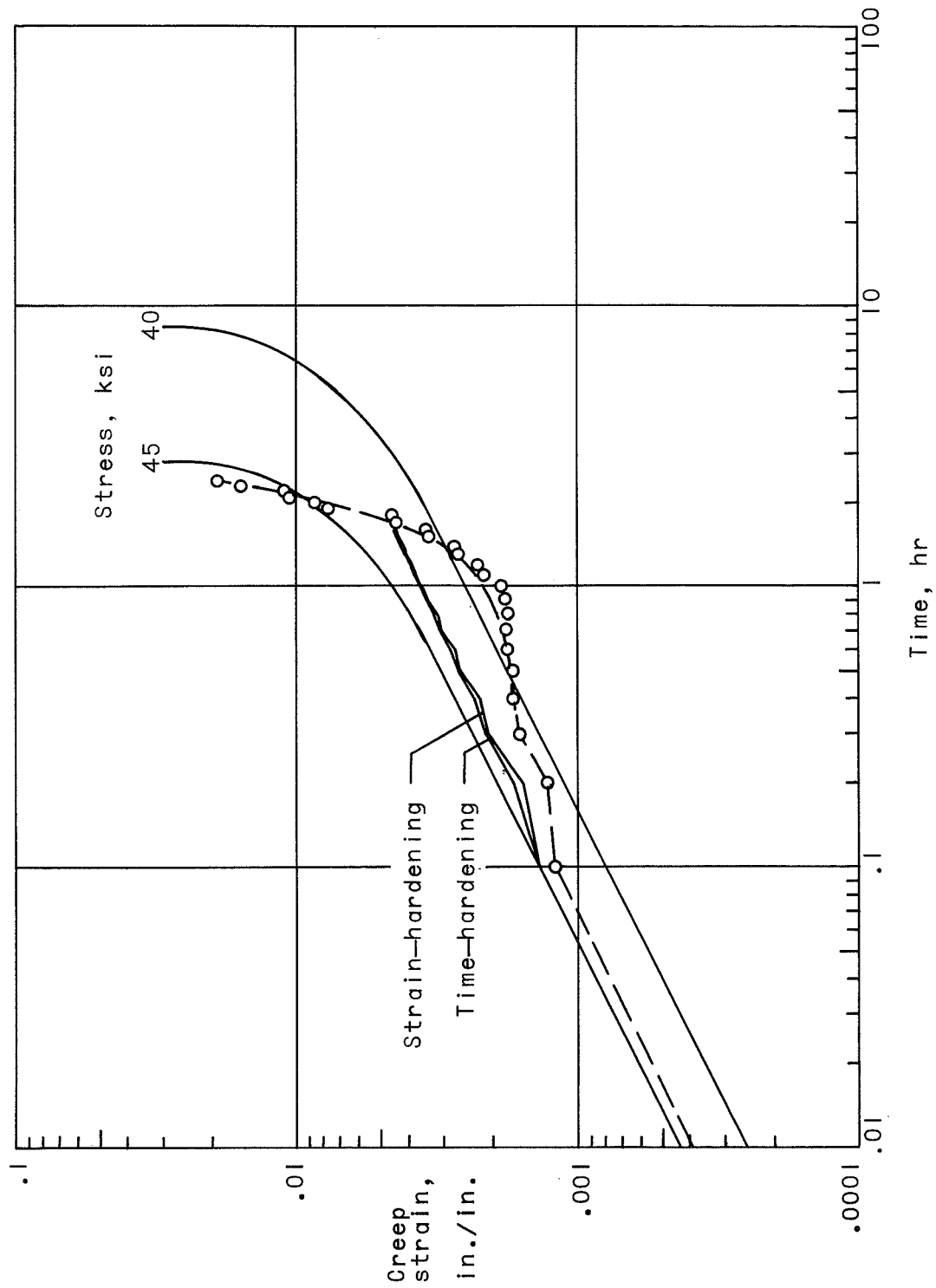Figure 12.- Multicyclic creep curves; test number 38.

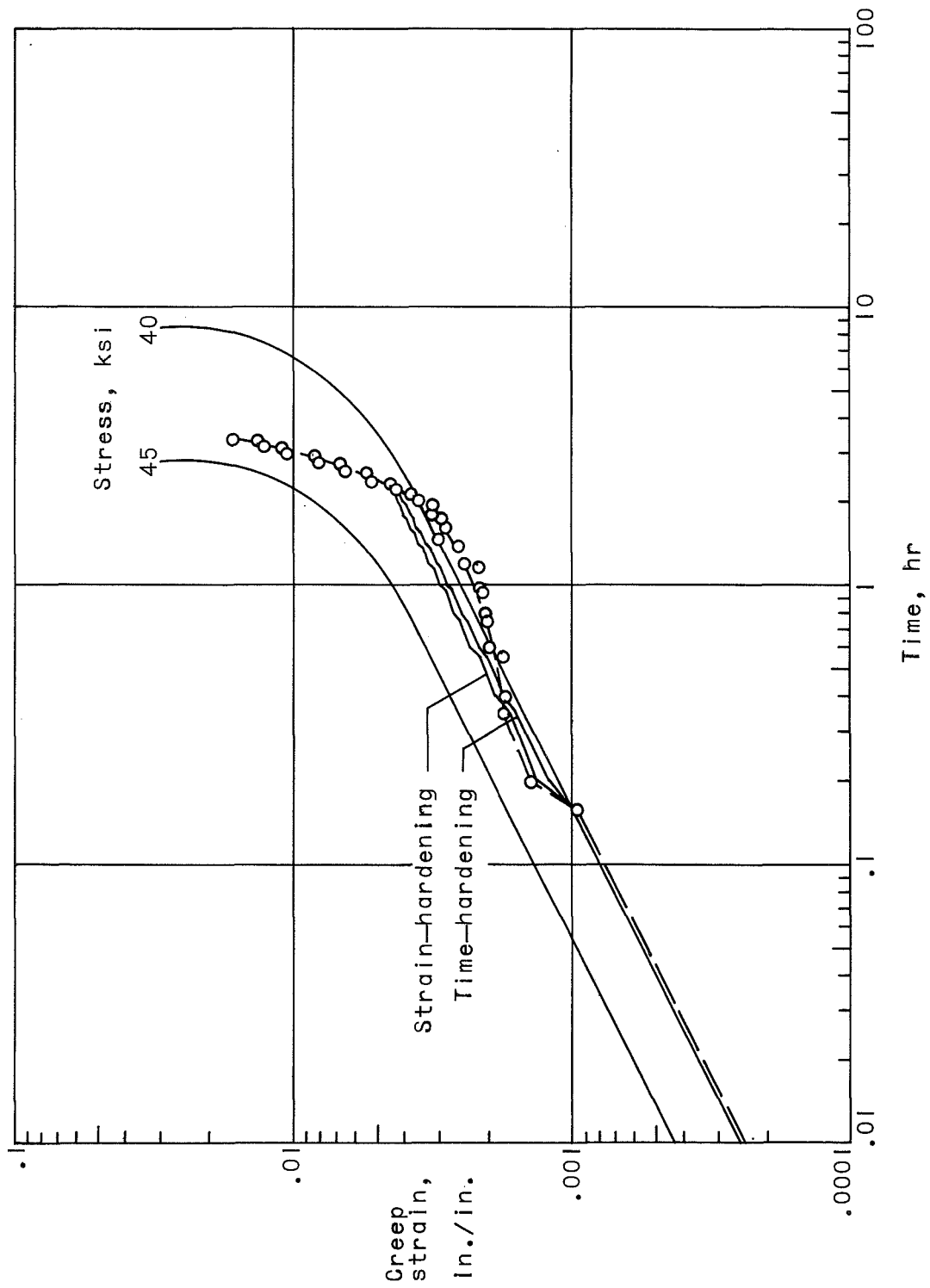Figure 13.- Multicyclic creep curves; test number 39.

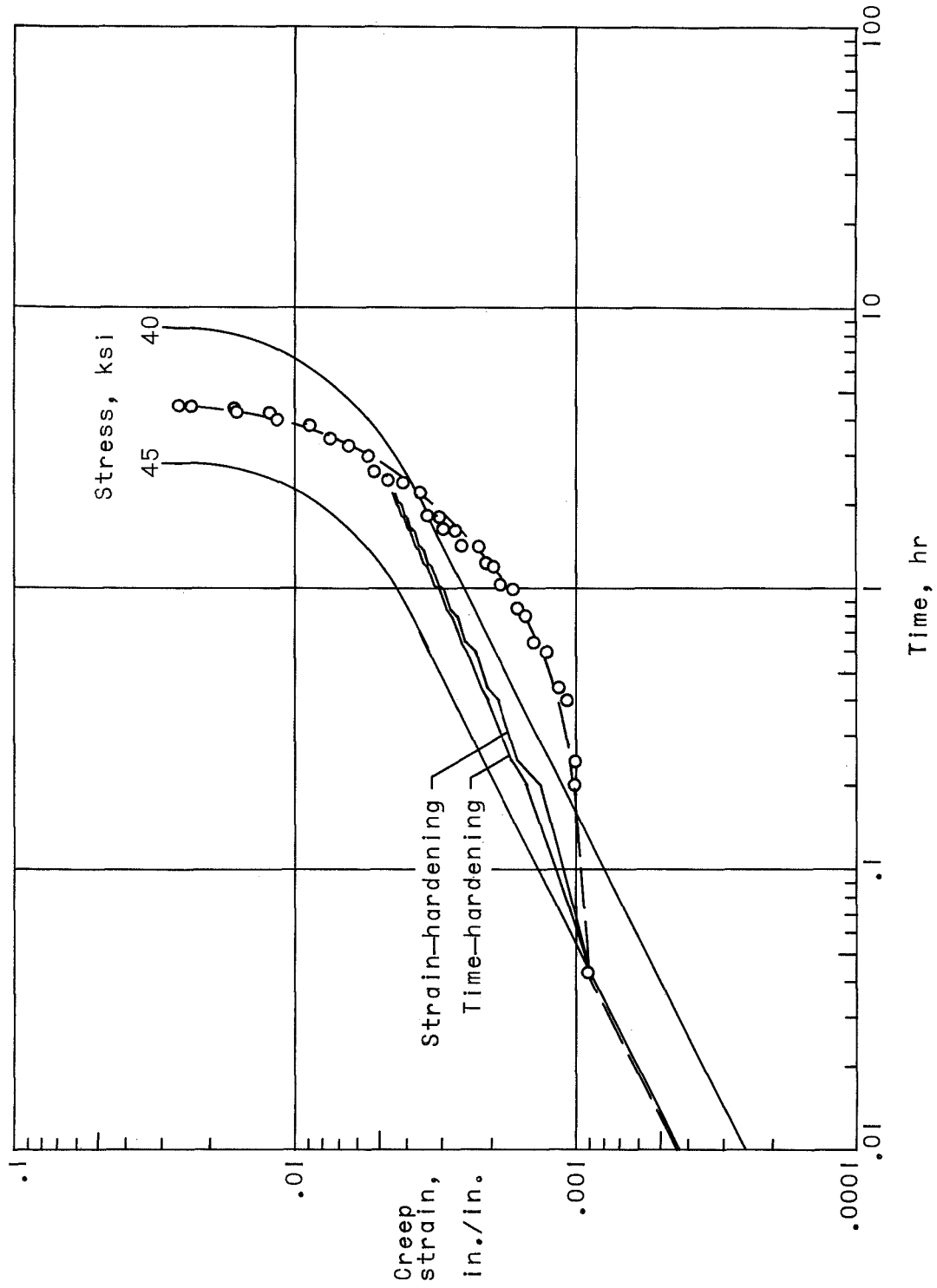Figure 14.- Multicyclic creep curves; test number 40.

Figure 15.- Multicyclic creep curves; test number 41.

Figure 16.- Multicyclic creep curves; test number 42.

Figure 17.- Multicyclic creep curves; test number 43.

Figure 18.- Multicyclic creep curves; test number 44.

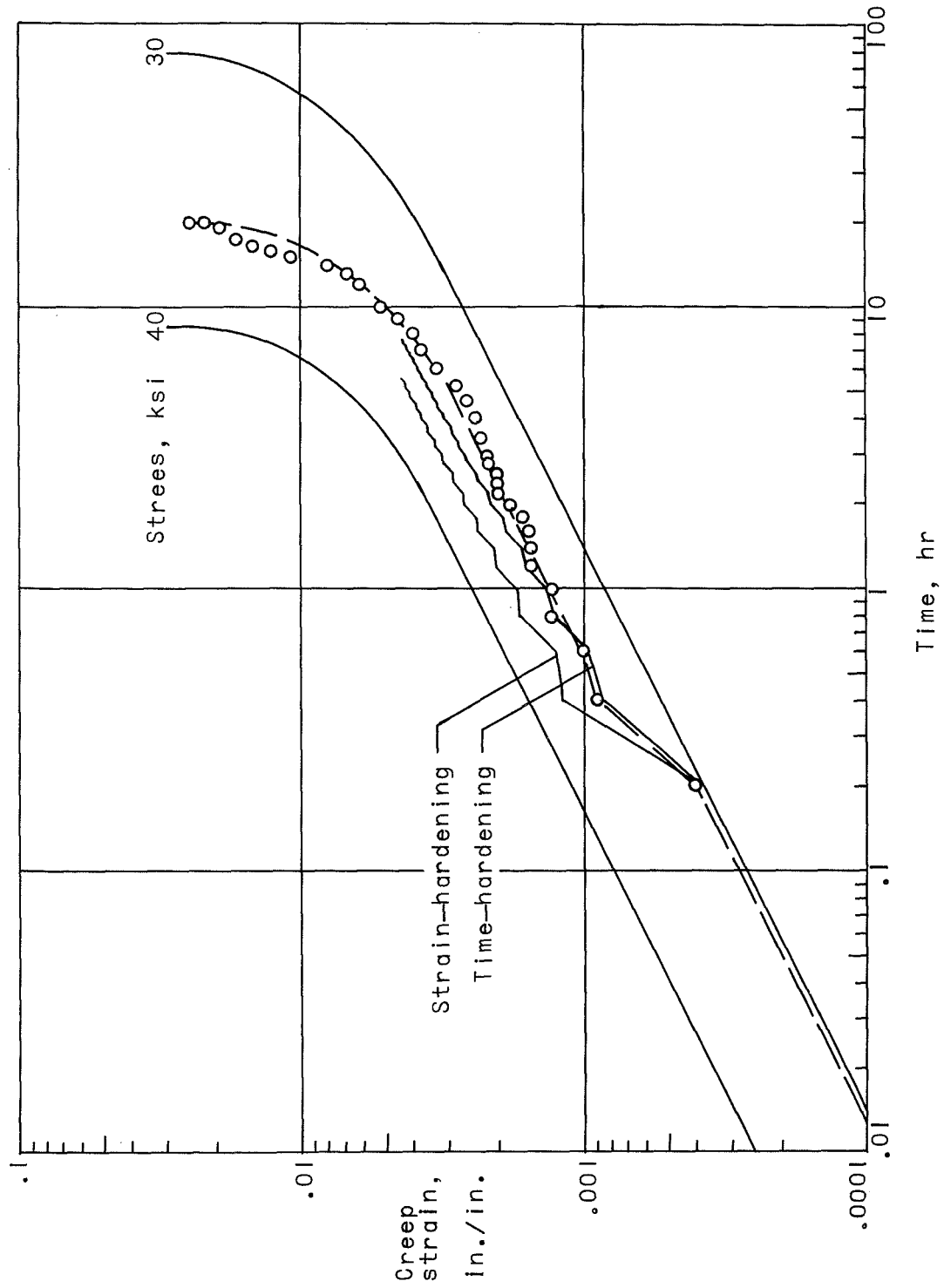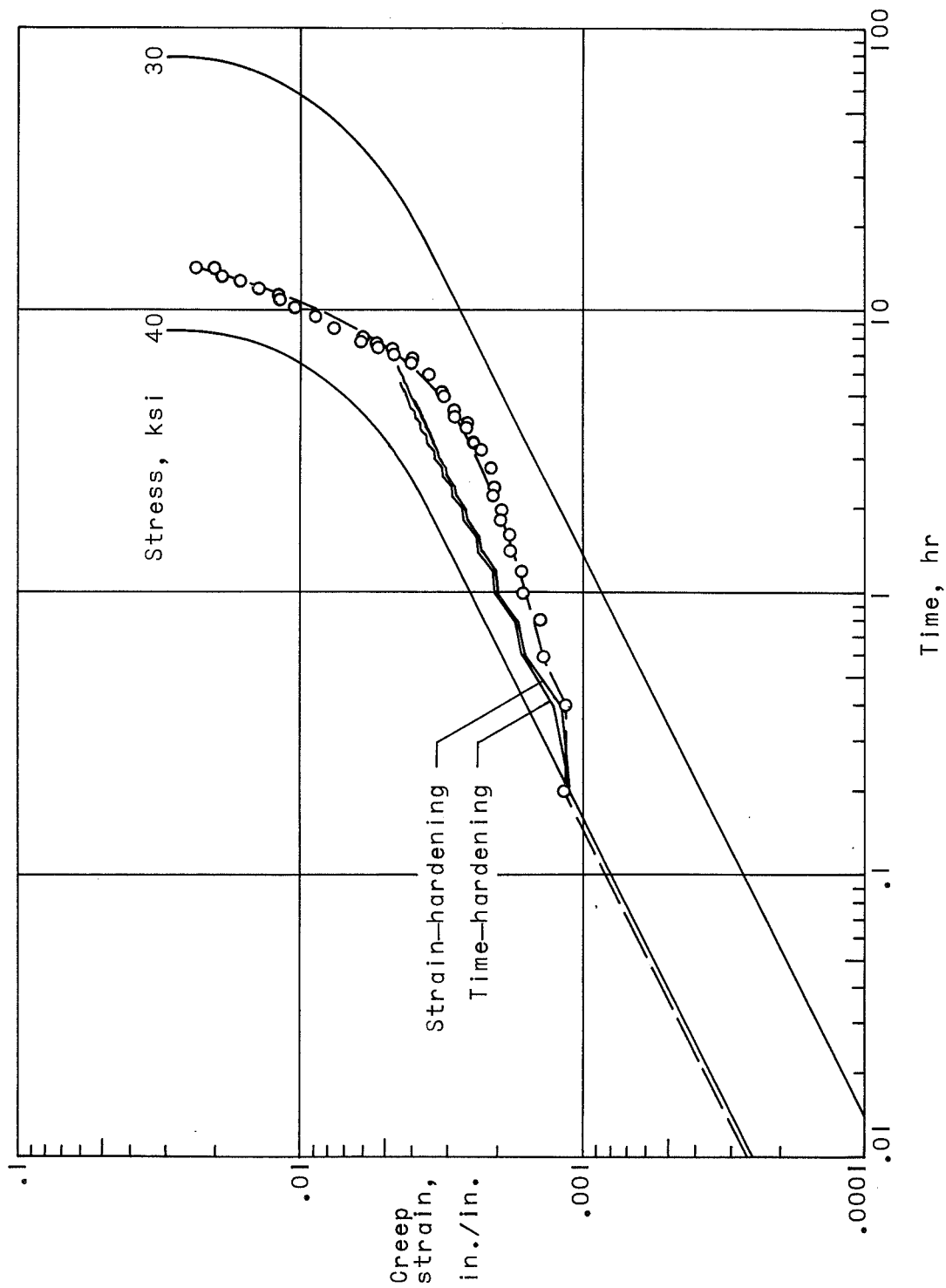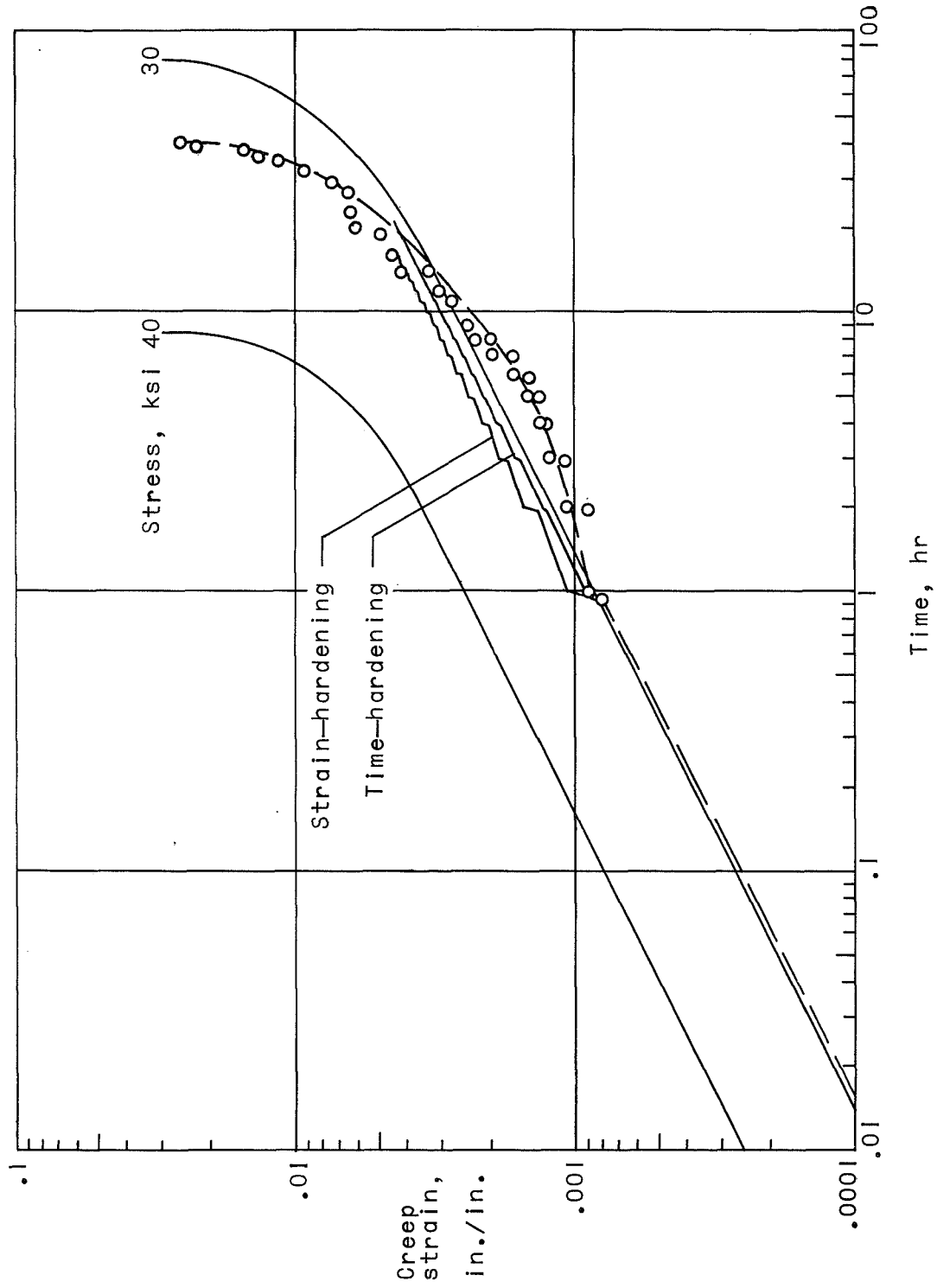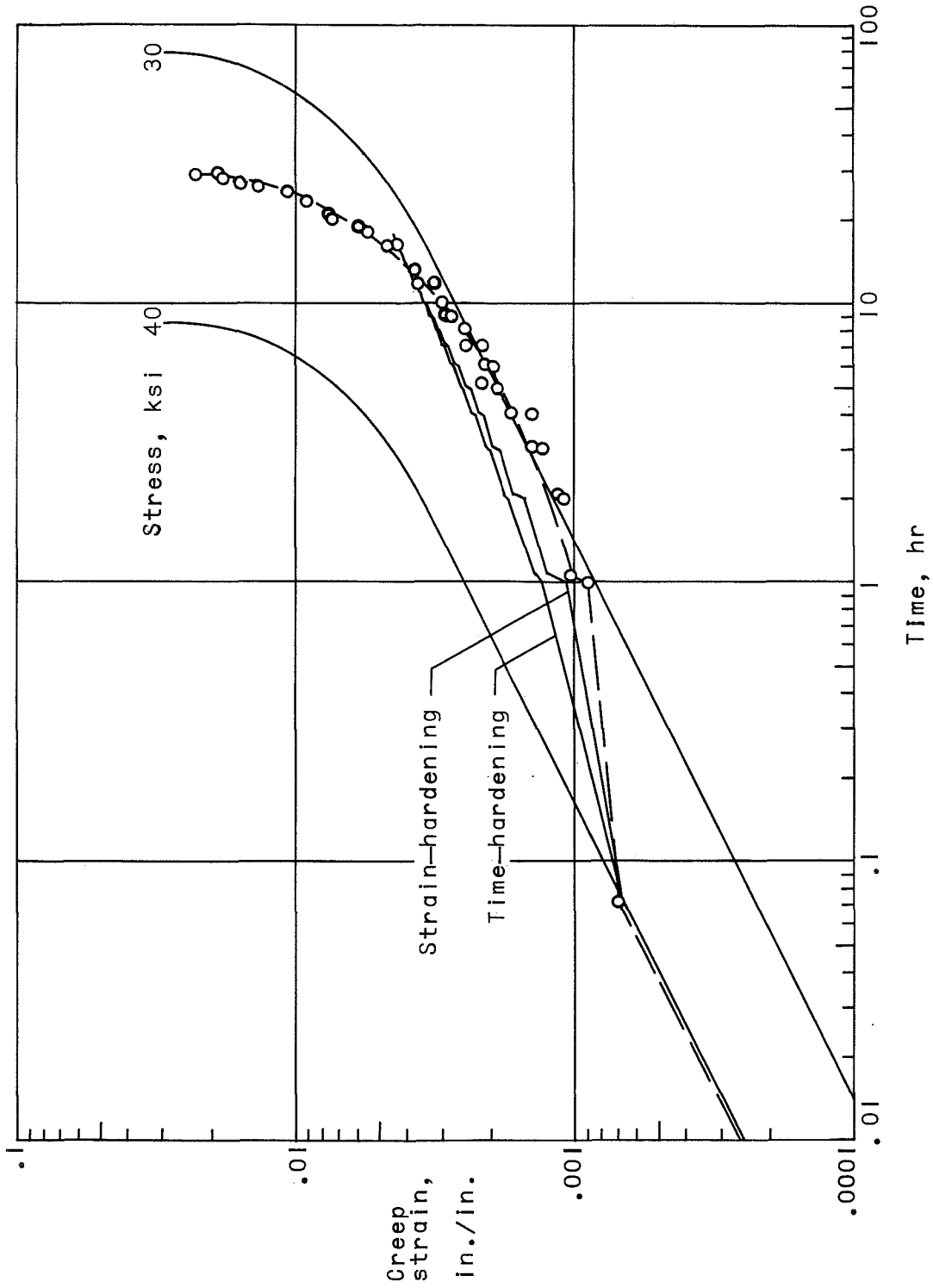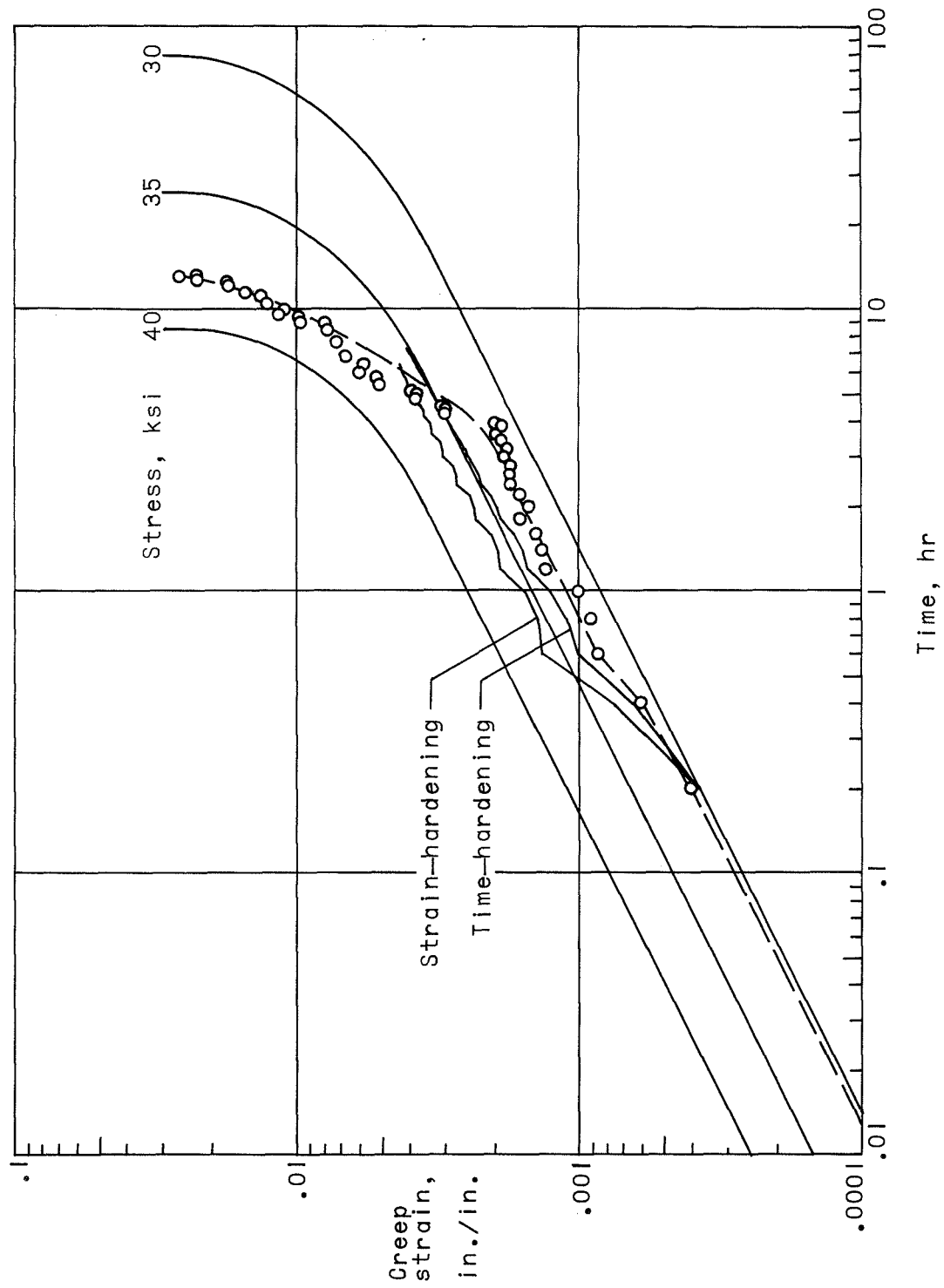Figure 19.- Multicyclic creep curves; test number 45.

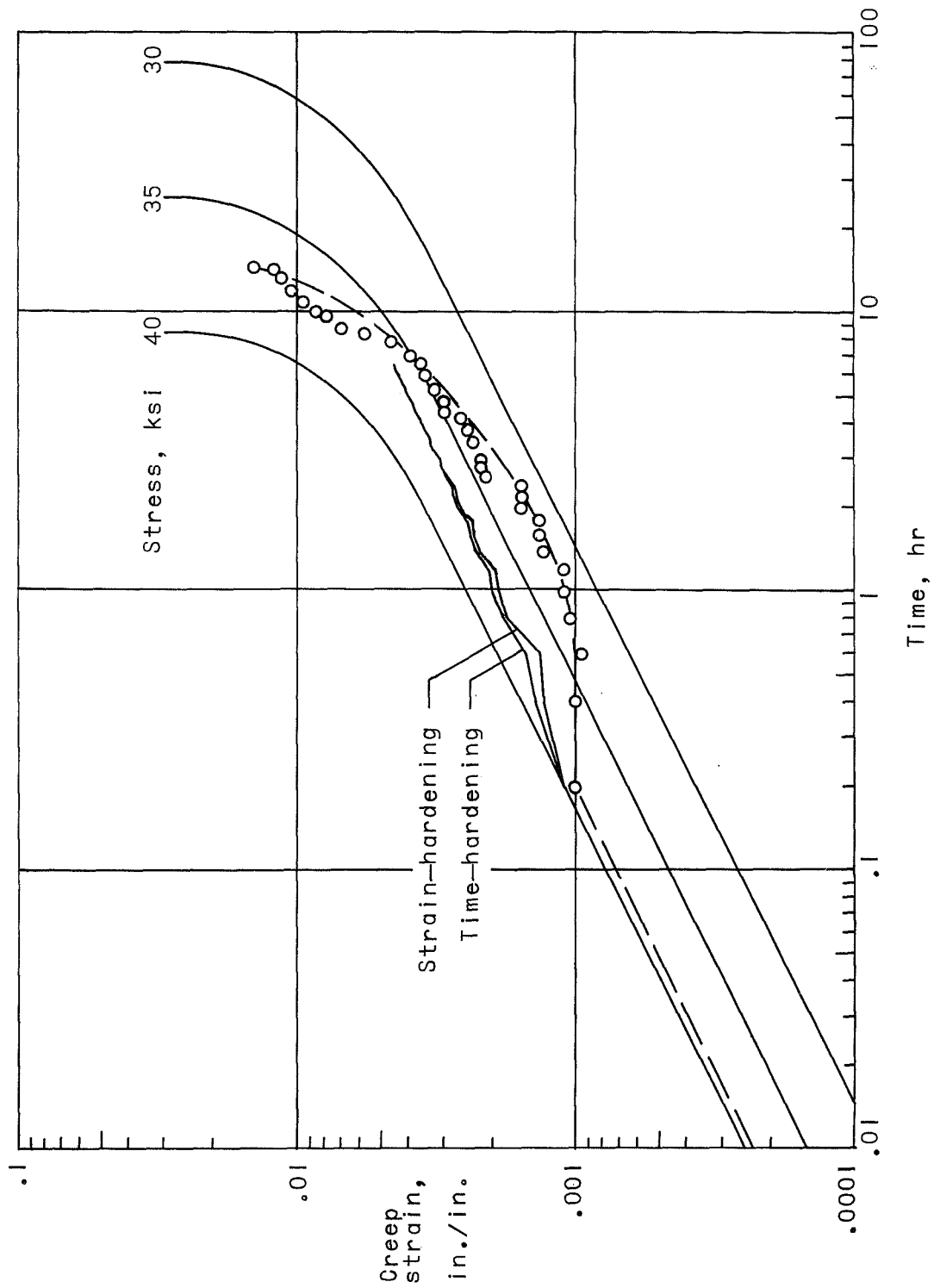Figure 20.- Multicyclic creep curves; test number 46.

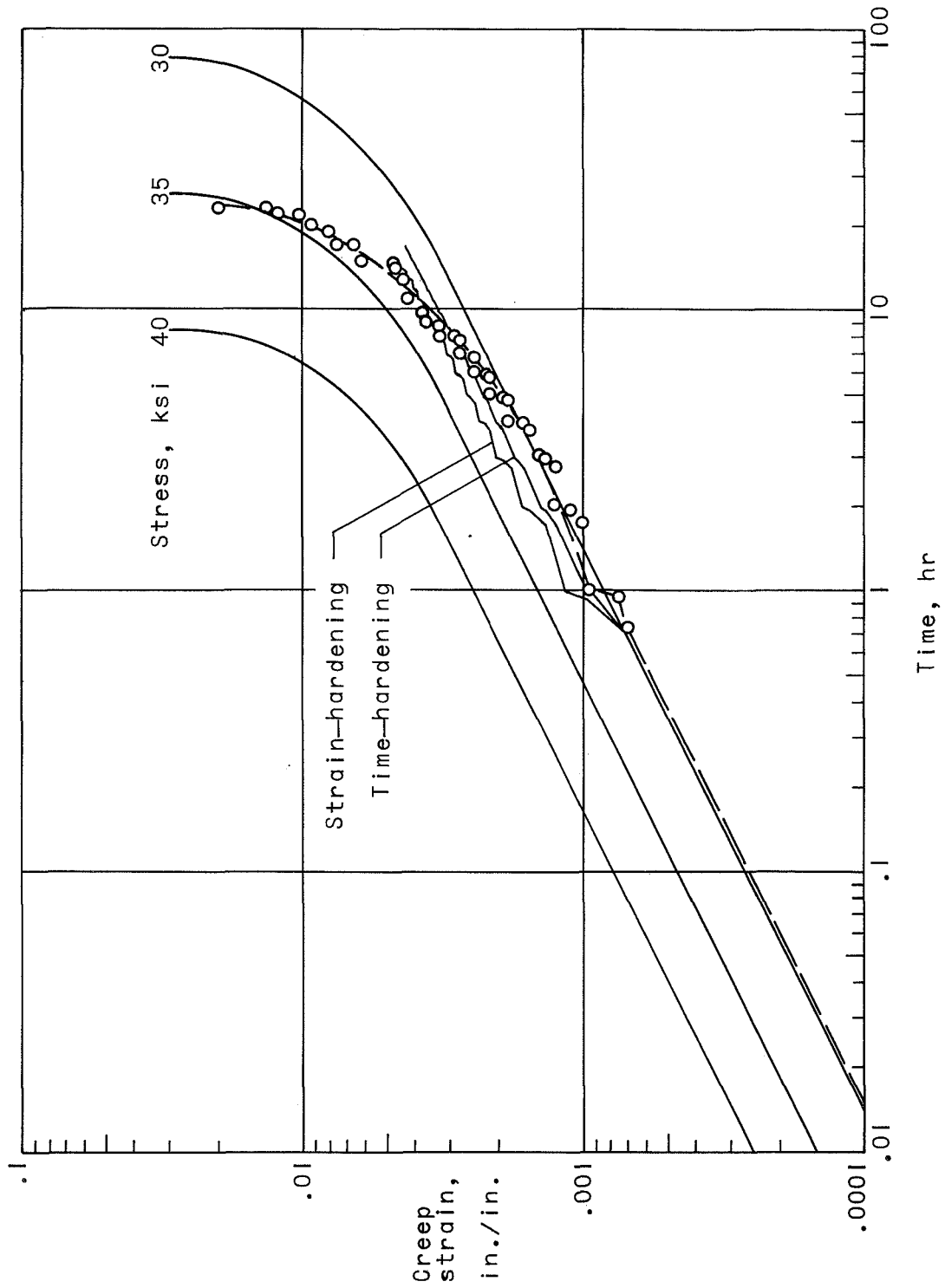Figure 21.- Multicyclic creep curves; test number 47.

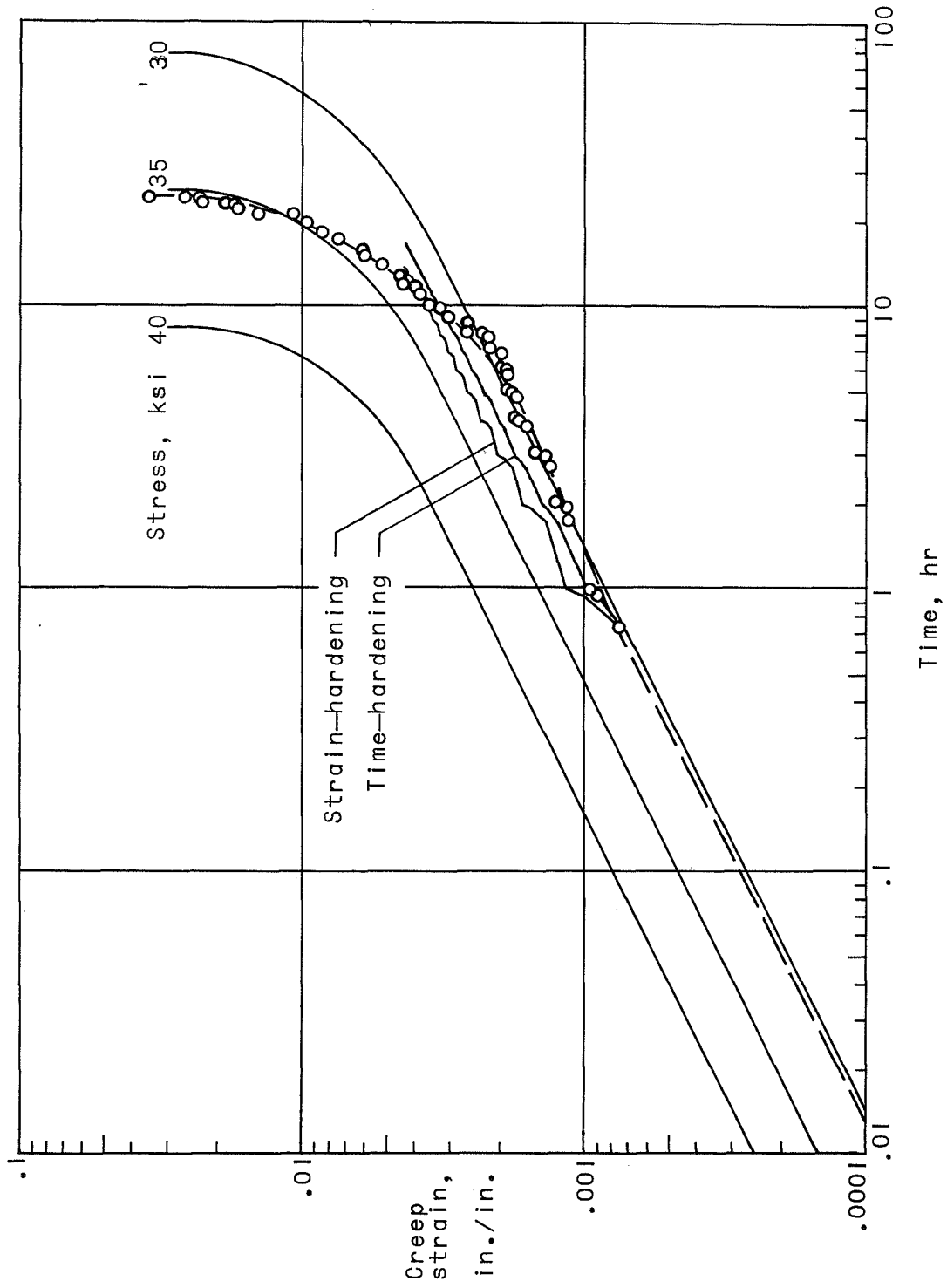Figure 22.- Multicyclic creep curves; test number 48.

Figure 23.- Multicyclic creep curves; test number 49.
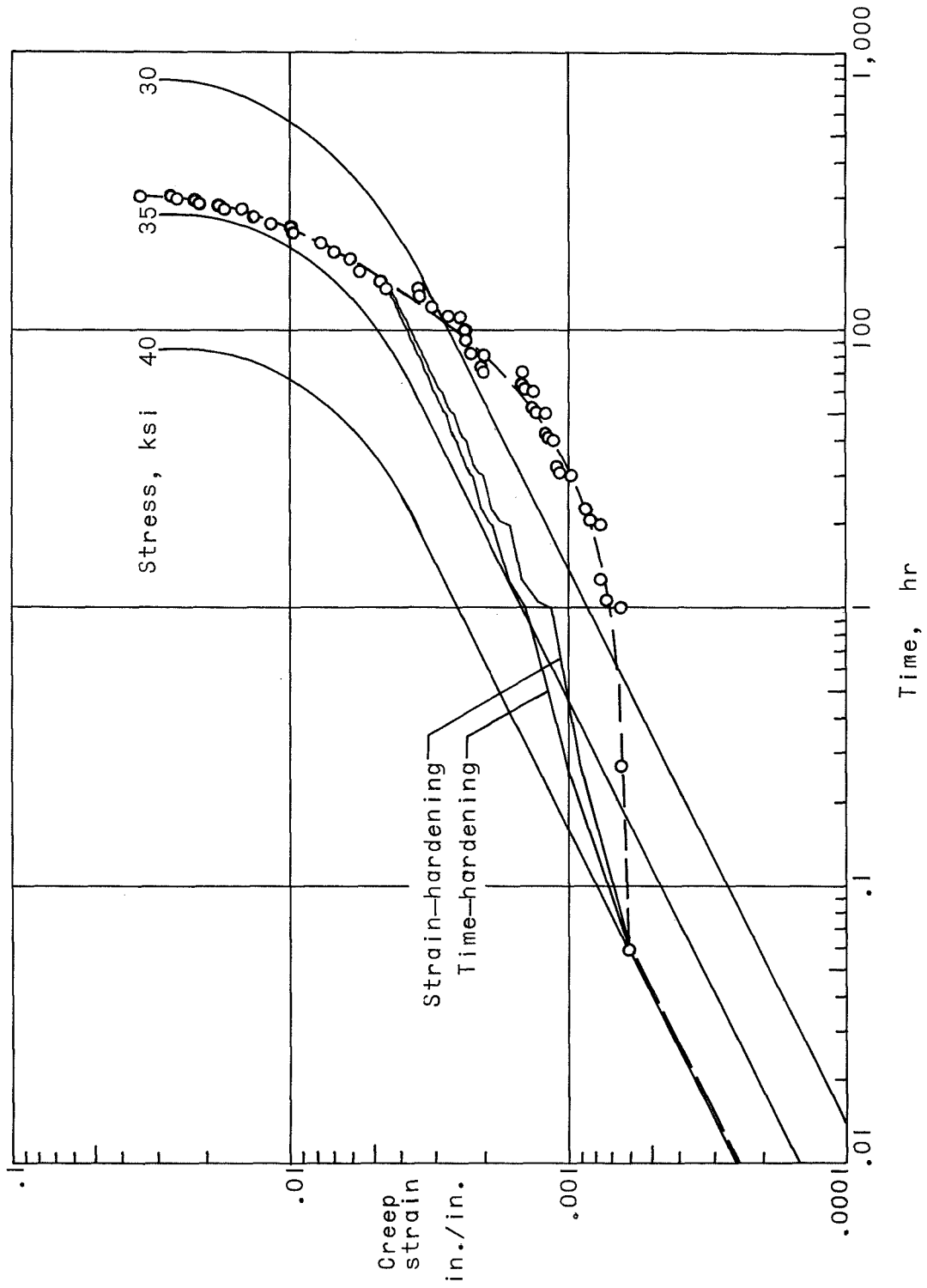
Figure 24.- Multicyclic creep curves; test number 50.

equations (7), (10), and (13). These equations are repeated here
with the values of the constants introduced for ease of reference.

Time-hardening theory:

$$\epsilon_1 = (6.8 \times 10^{-5}) \sum_{n=1}^{n=i} \left[(t_n^{1/2} - t_{n-1}^{1/2}) \sinh \frac{\sigma_n}{9.3} \right] \qquad (18)$$

Strain-hardening theory:

$$\epsilon_1 = (6.8 \times 10^{-5}) \left(\sum_{n=1}^{n=i} \Delta t_n \sinh^2 \frac{\sigma_n}{9.3} \right)^{1/2} \qquad (19)$$

Life-fraction rule:

$$\epsilon_1 = (6.8 \times 10^{-5}) t_1^{1/2} \sinh \frac{\sigma_1}{9.3} + (6.8 \times 10^{-5}) \sum_{m=2}^{m=i} \left\{ t_{rm}^{1/2} \left[\left(\sum_{n=1}^{n=m} \frac{\Delta t_n}{t_{rn}} \right)^{1/2} - \left(\sum_{n=1}^{n=m-1} \frac{\Delta t_n}{t_{rn}} \right)^{1/2} \right] \sinh \frac{\sigma_m}{9.3} \right\} \qquad (20)$$

In the light of equation (17) for the rupture times t_r certain
modifications can be made in equation (20). Writing equation (20)
more fully and substituting for the rupture times from equation (17)
one obtains

$$\epsilon_1 = (6.8 \times 10^{-5})\left\{ t_1^{1/2} \sinh \frac{\sigma_1}{9.3} + \left[\left(\Delta t_1 \frac{\sinh^2 \frac{\sigma_1}{9.3}}{\sinh^2 \frac{\sigma_2}{9.3}} + \Delta t_2 \right)^{1/2} - \right. \right.$$

$$\left. \left(\Delta t_1 \frac{\sinh^2 \frac{\sigma_1}{9.3}}{\sinh^2 \frac{\sigma_2}{9.3}} \right)^{1/2} \right] \sinh \frac{\sigma_2}{9.3} + \left[\left(\Delta t_1 \frac{\sinh^2 \frac{\sigma_1}{9.3}}{\sinh^2 \frac{\sigma_3}{9.3}} + \Delta t_2 \frac{\sinh^2 \frac{\sigma_2}{9.3}}{\sinh^2 \frac{\sigma_3}{9.3}} + \Delta t_3 \right)^{1/2} - \right.$$

$$\left. \left. \left(\Delta t_1 \frac{\sinh^2 \frac{\sigma_1}{9.3}}{\sinh^2 \frac{\sigma_3}{9.3}} + \Delta t_2 \frac{\sinh^2 \frac{\sigma_2}{9.3}}{\sinh^2 \frac{\sigma_3}{9.3}} \right)^{1/2} \right] \sinh \frac{\sigma_3}{9.3} + etc... \right\}$$

$$= (6.8 \times 10^{-5})\left\{ t_1^{1/2} \sinh \frac{\sigma_1}{9.3} + \left[\left(\Delta t_1 \sinh^2 \frac{\sigma_1}{9.3} + \Delta t_2 \sinh^2 \frac{\sigma_2}{9.3} \right)^{1/2} - \right. \right.$$

$$\left. \Delta t_1^{1/2} \sinh \frac{\sigma_1}{9.3} \right] + \left[\left(\Delta t_1 \sinh^2 \frac{\sigma_1}{9.3} + \Delta t_2 \sinh^2 \frac{\sigma_2}{9.3} + \Delta t_3 \sinh^2 \frac{\sigma_3}{9.3} \right)^{1/2} - \right.$$

$$\left. \left. \left(\Delta t_1 \sinh^2 \frac{\sigma_1}{9.3} + \Delta t_2 \sinh^2 \frac{\sigma_2}{9.3} \right)^{1/2} \right] + etc... \right\}$$

$$= (6.8 \times 10^{-5})\left(\Delta t_1 \sinh^2 \frac{\sigma_1}{9.3} + \Delta t_2 \sinh^2 \frac{\sigma_2}{9.3} + ... + \Delta t_i \sinh^2 \frac{\sigma_i}{9.3} \right)^{1/2}$$

$$= (6.8 \times 10^{-5})\left(\sum_{n=1}^{n=i} \Delta t_n \sinh^2 \frac{\sigma_n}{9.3} \right)^{1/2} \tag{21}$$

Equation (21) is identical with equation (19), which indicates that the strain-hardening and life-fraction laws are identical within the range of stress where both equation (4) for creep strain and equation (15) for rupture strain apply (cf., the "K"-factor method of refs. 4 and 25).

Theoretical values of creep strain are plotted against time in figures 12 through 24 with the aid of equations (18) and (19) up to a

creep strain of about 0.004 inch/inch. Beyond this value of creep strain
equation (4) no longer describes the basic creep curves accurately and
therefore equations (18) and (19) cannot be applied beyond that strain.
Strains predicted by the theoretical results were conservative in every
case, being more so in cases when the high stress was applied before
the lower stresses.

The effect of creep recovery apparently controlled the rate of
creep until a strain of approximately 0.0025 inch/inch had occurred,
the effect being stronger when the high loads were applied first. At
strains greater than 0.0025 inch/inch the strain rate increased until
failure of the specimen occurred.

2. Creep rupture.- The experimental creep curves of figures 12
through 24 end at the point of specimen rupture. The time at which
failure occurred in each test is recorded in table 5. In most of the
varied load tests failure occurred between the failure times of the
largest and smallest stresses applied during the test, and no consistent
difference in failure times could be found depending on the order of
application of load. The exceptions were the single cycle tests in
which the higher stress was applied first. In such cases rupture always
occurred well beyond the rupture time of the lower stress applied during
the test. As has been pointed out previously, this delay in rupture
time was caused by the recovery phenomenon which began to function when
the load was reduced.

A method for predicting the rupture time of a specimen under varying
load creep conditions is desirable. Since every varied load creep test
possesses a distinct rupture time, an equivalent rupture stress may be

TABLE 5.   RUPTURE DATA FOR CYCLIC LOAD CREEP TESTS

No.	σ_e, ksi	Rupture time, hr.
31	42.1	5.80
32	41.3	18.00
33	41.3	25.70
34	31.5	50.57
35	32.4	211.70
36	33.3	527.50
37	34.8	115.10
38	44.5	2.58
39	44.5	2.28
40	43.0	3.39
41	43.0	4.52
42	38.6	19.93
43	38.6	14.05
44	33.3	39.94
45	33.3	29.03
46	37.9	13.01
47	38.0	14.45
48	34.2	22.95
49	34.2	23.95
50	34.2	30.02

defined which is equal to the stress which when applied continuously would cause failure at the same time. Creep rupture data obtained at constant stress could then be used to determine rupture time under varying loads.

Expressions for the calculation of the equivalent rupture stress from the load-time cycle characteristics of varied load creep tests can be derived as follows by using the life-fraction rule. This rule states that failure occurs when

$$\sum_{n=1}^{n=i} \frac{\Delta t_n}{t_{rn}} = 1 \tag{22}$$

(see equation (11)). The time at which equation (22) is satisfied is

$$t_r = \sum_{n=1}^{n=i} \Delta t_n \tag{23}$$

Since failure must occur while stress σ_i is applied, Δt_i is not known. However, from equation (22)

$$\Delta t_i = t_{ri} \left(1 - \sum_{n=1}^{n=i-1} \frac{\Delta t_n}{t_{rn}} \right) \tag{24}$$

which when substituted into equation (23) gives a rupture time of

$$t_r = \sum_{n=1}^{n=i-1} \Delta t_n + t_{ri} \left(1 - \sum_{n=1}^{n=i-1} \frac{\Delta t_n}{t_{rn}} \right)$$

$$= \sum_{n=1}^{n=i-1} \Delta t_n \left(1 - \frac{t_{ri}}{t_{rn}} \right) + t_{ri} \tag{25}$$

Substituting for t_{rn} in equation (25) from equation (16) one obtains

$$t_r = \sum_{n=1}^{n=i-1} \Delta t_n \left(1 - \frac{\sinh^{1/k} \frac{\sigma_n}{\sigma_0}}{\sinh^{1/k} \frac{\sigma_i}{\sigma_0}} \right) + \frac{C}{\sinh^{1/k} \frac{\sigma_i}{\sigma_0}} \qquad (26)$$

The equivalent rupture stress σ_e is defined such that the calculated varied load rupture time is

$$t_r = C/\sinh^{1/k} \frac{\sigma_e}{\sigma_0} \qquad (27)$$

By combining equations (26) and (27) the equivalent rupture stress can be computed from the formula

$$\sinh \frac{\sigma_e}{\sigma_0} = \left[\frac{C \sinh^{1/k} \frac{\sigma_i}{\sigma_0}}{\sum_{n=1}^{n=i-1} \Delta t_n \left(\sinh^{1/k} \frac{\sigma_i}{\sigma_0} - \sinh^{1/k} \frac{\sigma_n}{\sigma_0} \right) + C} \right]^k \qquad (28)$$

In the case of the single cycle tests reported herein, for which only two load levels were used, equation (28), with the values of the constants substituted, becomes

$$\sinh \frac{\sigma_e}{9.3} = \sinh \frac{\sigma_2}{9.3} \sqrt{\frac{1.2 \times 10^4}{t_1 \left(\sinh^2 \frac{\sigma_2}{9.3} - \sinh^2 \frac{\sigma_1}{9.3} \right) + (1.2 \times 10^4)}} \qquad (29)$$

It will now be shown that an expression for the equivalent rupture stress which is simpler than that of equation (28) can be derived by consideration of the cycle characteristics in a repeated cycle test. For

the purpose of this derivation it must be assumed that failure of the specimen occurs at the end of one of the cycles. This assumption introduces very little error if many cycles are required to cause failure. In the case when the assumption is valid, equation (23) can be expressed as

$$t_r = N \sum_{m=1}^{m=j} \Delta t_m \tag{30}$$

where N is the number of cycles and j is the number of load steps per cycle. Equation (22) can now be expressed as

$$N \sum_{m=1}^{m=j} \frac{\Delta t_m}{t_{rm}} = 1 \tag{31}$$

so that equation (30) becomes

$$t_r = \sum_{m=1}^{m=j} \frac{t_{rm}}{\Delta t_m} \cdot \sum_{m=1}^{m=j} \Delta t_m \tag{32}$$

Substituting for t_{rm} in equation (32) from equation (16) one obtains

$$t_r = C \sum_{m=1}^{m=j} \frac{1}{\Delta t_m \sinh^{1/k} \frac{\sigma_m}{\sigma_o}} \cdot \sum_{m=1}^{m=j} \Delta t_m \tag{33}$$

Then by combining equations (33) and (27) the resulting expression for computing equivalent rupture stresses is

$$\sinh \frac{\sigma_e}{\sigma_o} = \left(\frac{\sum_{m=1}^{m=j} \Delta t_m \sinh^{1/k} \frac{\sigma_m}{\sigma_o}}{\sum_{m=1}^{m=j} \Delta t_m} \right)^k \tag{34}$$

Substituting for the constants k and σ_0 in equation (34) one obtains

$$\sinh \frac{\sigma_e}{9.3} = \left(\frac{\sum\limits_{m=1}^{m=j} \Delta t_m \sinh^2 \frac{\sigma_m}{9.3}}{\sum\limits_{m=1}^{m=j} \Delta t_m} \right)^{1/2} \tag{35}$$

Experimentally determined rupture times from the varied load creep tests are presented in table 5 and plotted in figure 25 against equivalent rupture stresses calculated with the aid of equations (29) and (35). The solid line in figure 25 gives the values of rupture time predicted by equation (17). As in the case of the constant stress creep rupture data (fig. 8), agreement between predicted and experimental values is good, with the exception of those single cycle tests in which the higher stress was applied first. Note, however, that the latter test points fall in a line parallel to that calculated from equation (17).
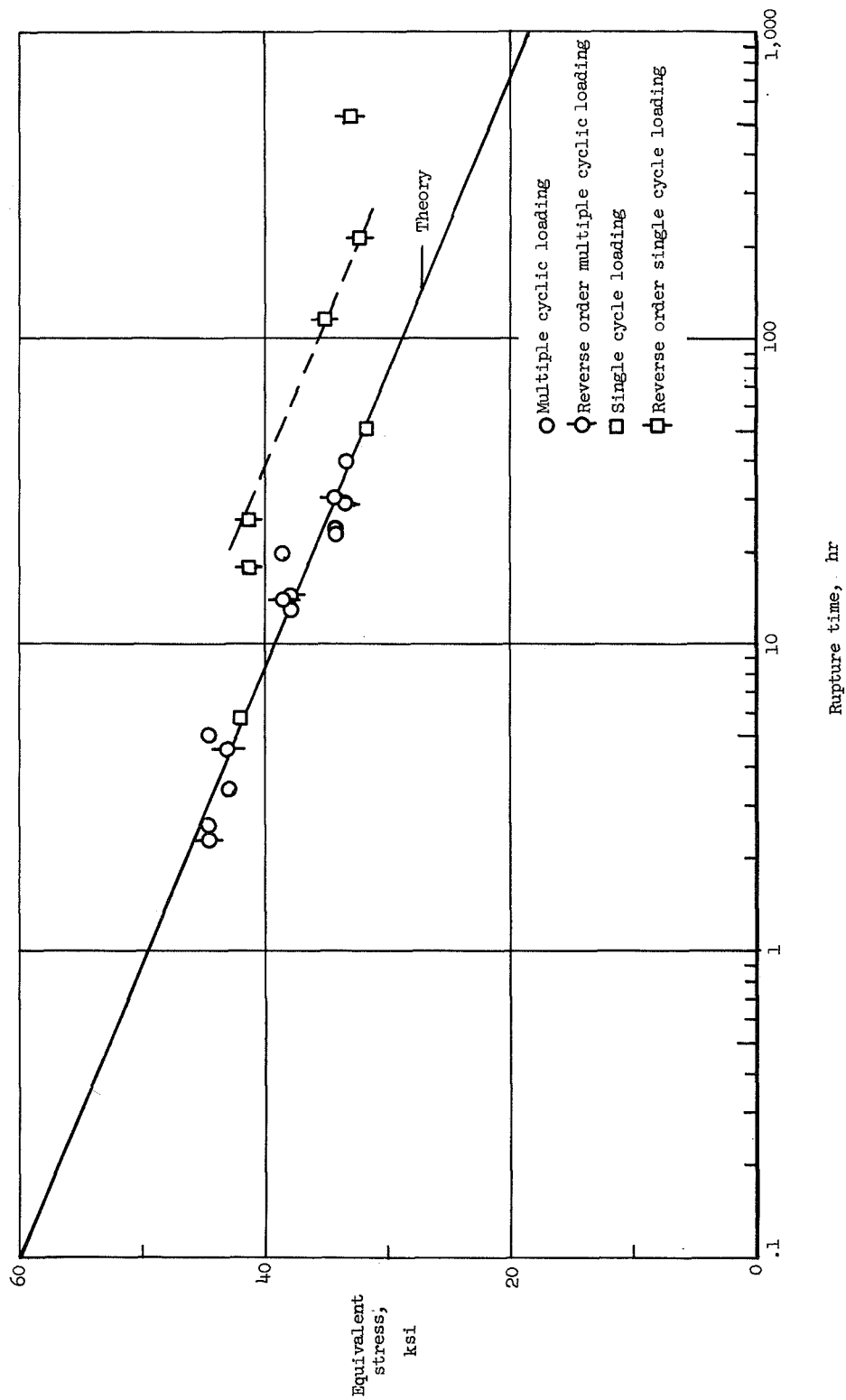
Figure 25.- Creep rupture time of 2024-T3 aluminum-alloy sheet at 400° F under cyclic loads.

X. CONCLUSIONS

Materials data have been presented on 2024-T3 aluminum-alloy
sheet in tension at 400° F, including the results of creep tests under
conditions of varying loads. Three theories, namely, a time-hardening
law, a strain-hardening law, and a life-fraction rule, have been applied
to predict the amount of primary and secondary creep strain to be expected
under varying load conditions, and were found to give conservative values
in every case investigated. This was due to the fact that the mechanism
of creep recovery, which acts when the applied stress has been decreased,
was dominant in the range of interest (up to approximately 0.002 inch/inch
creep strain).

The strain-hardening and life-fraction theories were shown to give
identical results if the empirical expression describing the primary and
secondary stages of the constant load creep curves and that describing
the creep strain at rupture are of the same form.

An equation was developed using the life-fraction rule by which an
equivalent rupture stress can be calculated for creep tests under repeated
cyclic loads. Creep rupture times were predicted with satisfactory
accuracy using the equivalent rupture stresses and the creep rupture
curve determined from constant load tests.

The results appear to be independent of the order of loading if
many load cycles are required to fail the specimen. In the case of
single cycle tests the equivalent stress method proved satisfactory when
the tests were begun at the lower stress; the method was very conservative
when the opposite order of loading was applied.

The results of this investigation show that much more must be learned concerning the mechanism of creep and in particular creep recovery before the latter can be applied quantitatively to help solve problems of this nature on the engineering level.

XI.   ACKNOWLEDGEMENTS

XII. REFERENCES

1. Symposium on Effect of Cyclic Heating and Stressing on Metals at Elevated Temperatures. June 17, 1954. ASTM Special Technical Publication no. 165, 1954.

2. Guarnieri, G. J., and Yerkovich, L. A.: Influence of Periodic Overstressing on the Creep Properties of Several Heat Resistant Alloys. Proceeding of ASTM, vol. 52, 1952, p. 934.

3. Rabotnov, Y. N.: The Effect of Changing Loads During Creep. Creep and Fracture of Metals at High Temperature, National Physical Laboratory, London, 1956.

4. Isaksson, Åke: Krypning vid Variabel Spänning och Temperatur Bibliographi. (Bibliography on Creep Under Variable Stress and Temperature.) Division of Strength of Materials, Royal Inst. of Tech., Stockholm, Publication No. 116, 1957.

5. Mathauser, Eldon E., Berkovits, Avraham, and Stein, Bland A.: Recent Research on the Creep of Airframe Components. NACA TN 4014, 1957.

6. Goldin, Robert: Thermal Creep Design Criteria. Institute of the Aeronautical Sciences Preprint no. 730, 1957.

7. Marin, Joseph: Engineering Materials, Their Mechanical Properties and Applications, ch. 6. Prentice-Hall, Inc., New York, 1952.

8. Nadai, A.: The Creep of Metals Under Various Stress Conditions. von Kármán Anniversary Volume, Calif. Inst. of Tech., 1941, p. 237.

9. Davis, Evan A.: Creep and Relaxation of Oxygen-Free Copper. Journal of Applied Mech., vol. 10, 1943, p. A-101.

10. Stowell, Elbridge Z.: A Phenomenological Relation Between Stress, Strain Rate, and Temperature for Metals at Elevated Temperatures. NACA Rept. 1343, 1958. (Supersedes NACA TN 4000.)

11. Jackson, L. R., Schwope, A. D., and Shober, F. R.: Summary Report on Information on the Plastic Properties of Aircraft Materials and Plastic Stability of Aircraft Structures at High Temperatures to the Rand Corporation. Battelle Mem. Inst., Dec. 15, 1949.

12. Mathauser, Eldon E., and Develkis, William D.: Investigation of Compressive Strength and Creep Lifetime of 2024-T3 Aluminum-Alloy Plates at Elevated Temperatures. NACA Rept. 1308, 1957. (Supersedes NACA TN 3552.)

13. Develkis, William D.: Investigation of the Compressive Strength and Creep of 7075-T6 Aluminum-Alloy Plates at Elevated Temperatures. NACA TN 4111, 1957.

14. Findley, William N., and Khosla, Gautam: Application of the Super-position Principle and Theories of Mechanical Equation of State, Strain and Time Hardening to Creep of Plastics Under Changing Loads. Journal of Applied Phys., vol. 26, 1955, p. 821.

15. Soderberg, C. Richard: The Interpretation of Creep Tests for Machine Design. Trans. of ASME, vol. 58, p. 733, 1936.

16. Mendelsohn, A., Hirschberg, M. H., and Manson, S. S.: A General Approach to the Practical Solutions of Creep Problems. ASME Annual Meeting, Paper no. 58 - A - 98, 1958.

17. Davenport, C. C.: Correlation of Creep and Relaxation Properties of Copper. Journal of Applied Mech., vol. 5, p. A-55, 1938.

18. Palmgren, Arvid: Die Lebensdauer von Kugellagern. (The Lifetime of Ball-Bearings.) Zeitschrift des Vereines deutscher Ingenieure, vol. 68, 1924, p. 339.

19. Miner, Milton A.: Cumulative Damage in Fatigue. Journal of Applied Mech., vol. 12, p. A-159, 1945.

20. Sully, A. H.: Recent Advances in Knowledge Concerning the Process of Creep in Metals. Progress in Metal Physics, vol. 6, p. 135, edited by Chalmers, B., and King, R. Pergamon Press Ltd., London and New York, 1956.

21. Schoeck, Gunther: Theory of Creep. Creep and Recovery, p. 199, ASTM, 1957.

22. Kuhlmann, Doris: On the Theory of Plastic Deformation. Proc. of the Phys. Soc., vol. 64, p. 140, 1951.

23. Kennedy, A. J.: Creep and Recovery in Metals. British Journal of Applied Phys., vol. 4, p. 225, 1953.

24. Mathauser, Eldon E.: Compressive Stress-Strain Properties of 2024-T3 Aluminum-Alloy Sheet at Elevated Temperatures. NACA TN 3853, 1956.

25. Daniels, N. H. G., Masuda, H. B., and Dorn, John E.: The Creep Properties of Metals Under Intermittent Stressing and Heating Conditions. WADC Tech. Rep. 53-336, Part 4, 1956.

XIII. VITA

The author was born in Berlin, Germany on October 28, 1934. He attended schools in London and Leeds, England, and graduated from Sydney Boys' High School, Sydney, Australia in December 1950. After spending 2-1/2 years at theological colleges and at Brooklyn College night school in New York City, New York, the author enrolled in the College of Industrial Technology of Boston University, Boston, Massachusetts. In September 1954 he transferred to the Massachusetts Institute of Technology, Cambridge, Massachusetts, whence he received the Degree of Bachelor of Science in Mechanical Engineering in June 1956. Upon graduation he accepted a position with the Structures Research Division of the National Advisory Committee for Aeronautics (now National Aeronautics and Space Administration), Langley Field, Virginia where he is now employed as an Aeronautical Research Engineer. In the spring of 1958 he entered Virginia Polytechnic Institute to commence studies toward the Degree of Master of Science in Engineering Mechanics. He is married.